Effect of combined translation and torsion on undrained uplift capacity of plate anchors: plastic limit analysis (PLA) solution

Hamid Reza Nouri[1], Giovanna Biscontin[2] and Charles P. Aubeny, M. ASCE[3]

ABSTRACT

Uplift capacity of plate anchors have been the focus of numerous studies, since anchor plates are designed for pull-out in normal operating conditions. However, the response of plate anchors under six-degrees-of-freedom loading caused during extreme loading conditions is poorly understood. The purpose of this study is to propose a simple yet sufficiently accurate analytical solution to investigate the behavior of plate anchor under combined in-plane translation and torsion and to evaluate its effect on the plate uplift bearing capacity. To this end, a modified plastic limit analysis (PLA) approach is introduced and compared with limit equilibrium (LE) and simplified upper bound baseline solutions. The proposed method is verified with three dimensional finite element (3D-FE). The variables considered in this study include plate aspect ratio, plate thickness, as well as load direction and eccentricity. Results of analytical solutions indicate the insensitivity of the "shape" of the shear-torsion yield envelope to plate thickness. This finding facilitates the use of simplified yet reasonable yield envelope for infinitely thin plate obtained from simplified PLA approach for other plate thicknesses. The "size" of the failure envelope (controlled by pure torsional and translational capacity) could be predicted fairly accurately by PLA and LE methods. Combination of these analytical methods offers a simple yet reasonably accurate solution to describe shear-torsion response of anchor plate. The obtained shear-torsion yield envelope is then fitted in the generalized six-degrees-of-freedom yield surface which describes the reducing effect of moment, torsion, and planar forces on the uplift capacity of plate.

KEY WORDS: plate anchor, torsional and translational bearing capacity, plastic limit analysis, limit equilibrium, finite element analysis, yield envelope.

---

[1] Senior Geotechnical Engineer, Shannon and Wilson, Inc., 400 North 34th Street Suite 100, P.O. Box 300303 Seattle, Washington, USA 98103. Ph.: +1 (206) 695-6924, E-mail: Nouri.hreza@gmail.com; hrn@shanwil.com
[2] University Lecturer in Geotechnical Engineering, University of Cambridge, Department of Engineering, Schofield Centre, High Cross, Madingley Road, Cambridge, UK CB3 0EL. Ph.: +44 (1223) 768-044, E-mail: gb479@cam.ac.uk
[3] Professor, Texas A&M University, Civil Engineering CE/TTI, 3136 TAMU, College Station, TX 77843-3136, USA. Ph.: (979) 845-4478, E-mail: caubeny@civil.tamu.edu

INTRODUCTION

In recent years the growing trend in searching and developing hydrocarbon reserves has forced offshore oil and gas industry into deep and ultra deep water. It becomes increasingly difficult and costly to keep the natural period of traditional fixed jacket or gravity-based structures below the dominant frequency of the sea wave spectrum in water depths exceeding 500 m (Aubeny et al. 2001). Thus, floating structures anchored to the seabed using catenary or taut-wire moorings has taken the place of conventional platforms (Aubeny et al. 2001). Plate anchors are increasingly being used to moor large floating offshore structures in deep and ultra deep water.

Plate anchors are installed to impart substantial uplift loading in normal operating conditions. However, they could be subjected to six-degrees-of-freedom general loading as well. The recent hurricane events in the Gulf of Mexico resulted in partial failure and drift of 17 deepwater Mobile Offshore Drilling Units (MODUs) in hurricanes Ivan, Katrina, and Rita. The drift of the platform causes a significant change in the orientation and amount of the resultant force, which appears as a substantial out-of-plane force acting on the anchor of the intact line. This could lead to substantial reduction in uplift capacity of the plate, failure of the anchor, and catastrophic damages to adjacent oil and gas infrastructure through colliding with other exploration and production platforms and rupturing the network of oil and gas pipelines by dragging anchors of the failed line on the seabed. Importance of understanding the plate anchor response under out-of-plane loading is not limited to design considerations under extreme loading conditions. It is a frequent practice for operators to work on two close wells in the same field. Instead of relocating the drilling unit and its mooring system, it is more efficient to winch between wells on one mooring system without removing and reinstalling anchors. If the wells are far enough, anchors will be subjected to out-of-plane loading.

The undrained uplift bearing capacity of deeply embedded plates has been the focus of the majority of previous studies, while the plate bearing capacity under general loading conditions has received considerably less attention. The purpose of this study is to develop adequately accurate yet simple analytical solutions to quantify the decreasing effect of translation and torsion on pull-out bearing capacity of plate anchors. These simplified approaches are more attractive solutions for practical purposes compared to expensive numerical simulation.

This study idealizes the geometry of the plate anchor as a rectangular plate of length L, width W and thickness t subjected to eccentric loading (Fig. 1): L is taken as the shorter dimension, aligned with the x-axis. Also assuming a homogeneous condition for soil, any spatial variation of soil parameters is neglected in this study (i.e. constant undrained shear strength). In general, any eccentricity angle ψ or load angle γ may occur. First, a number of simple baseline solutions for pure translation ($e = 0$ or $\gamma = 90°$), and pure torsion ($\gamma \neq 90°$and $e = \infty$) are derived from limit equilibrium (LE). For general conditions of eccentricity and load orientation for infinitely thin plate, a semi-analytical upper-bound limit analysis based approach is proposed. For a plate of finite thickness under general eccentric load, a more powerful method is required. To this end, the upper-bound plastic limit analysis (PLA) proposed by Yang et al. (2010) for infinitely thin plates is adopted and modified to better predict the bearing capacity for plates with finite thickness. The accuracy of the baseline solutions and PLA approach are evaluated through comparisons to three-dimensional finite element solutions. The proposed analytical solutions are used to develop a simplified approach to incorporate the shear-torsion interaction equation in the generalized yield envelope for plate anchor under six-degrees-of-freedom loading condition. The complete generalized yield surface is used to evaluate the uplift capacity of anchor plates under combined eccentric translational/planar forces and out-of-plane moments.

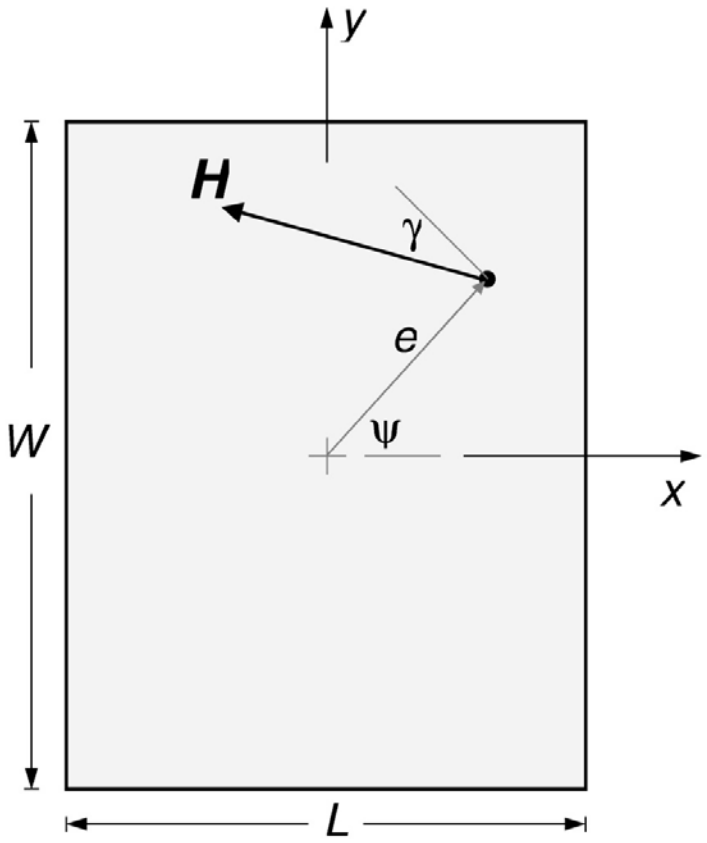

Figure 1- Schematic of eccentrically loaded plate

BACKGROUND

The majority of previous studies concerning the bearing capacity of plates are focused on undrained uplift capacity and limited literature is available on the bearing capacity of plate anchors subjected to general loading condition. O'Neill et al. (2003) used two-dimensional finite element (2D-FE) analysis to investigate the behavior of rectangular and wedge-shaped strip anchors subjected to combined translational, vertical, and rotational loadings. They also developed plastic upper bound solutions to evaluate plane strain ultimate parallel, normal, and rotational plate capacity factors to validate the FE results. They produced FE based yield surfaces and developed an approach to predict the kinematics and trajectory of drag anchor during the installation. Murff et al. (2005) used 2D-FE to develop yield loci for plates of

different thickness and roughness. Yang et al. (2010) employed 3D-FE, as well as plastic upper bound limit analysis, to study the behavior of infinitely thin plates subjected to six-degrees-of-freedom loading. They also introduced a plasticity solution to determine yield loci of an infinitely thin plate under combined translation-torsion. They developed equations to calculate pure sliding and torsional bearing capacity. Nouri (2013) conducted 3D-FE analysis to evaluate the response of plate anchors with finite thickness under in-plane two-way translation and torsion. Their 3D-FE results indicated the insensitivity of the shape of yield envelope (i.e. plate interaction response under combined loading) to thickness variations of square and rectangular anchors.

Yang et al. (2010) Upper Bound PLA Solution: Overview

Yang et al. (2010) developed an upper bound plastic limit analysis (PLA) formulation for deeply embedded square and rectangular plate anchors under combination of co-planar sliding and torsion. They assumed deep embedment for the plate anchor, which ensures “no separation” of undrained cohesive soil in contact with the foundation. The full attachment of the foundation and soil complies with the normality concept (Tan, 1990) which is essential to apply the limit analysis approach in soils (Chen and Liu, 1990). This assumption seems valid since due to the low permeability of clays in combination with a high loading rate, suction will be generated on faces of the plate (Wang et al. 2010).

In their approach a plate is assumed subjected to a force, F, in the plane parallel to the plate faces, passing through its center (Fig. 2). If the plate is subjected to a virtual rotation rate, $\dot{\beta}$, around point O(x_o, y_o), F could be calculated by equating the work done by external force, F, and the total rate of energy dissipation in the vicinity of plate failure:

$$F = \frac{\dot{D}_s + \dot{D}_e}{\left[\left(x_f - x_o\right)\cos\phi + \left(y_f - y_o\right)\sin\phi\right]\dot{\beta}} \quad (1)$$

where the total rate of energy dissipation is equal to the rate of energy dissipated by sliding along the top and bottom surfaces of the plate ($\dot{D}_s$) in addition to the rate of energy dissipated by the soil resistance on the plate edges ($\dot{D}_e$) (see Appendix A), and ϕ=ψ+γ is the angle between line of action of the external force and *y*-axis. The minimum value for the force, *F*, can be determined by optimizing the kinematics of the plate rigid body motions with respect to the coordinates of the rotation center of the rotating plate, O(x_o, y_o). The pure sliding (shear loading) occurs when the line of action of the force, *F*, is passing through the center of the plate and pure torsion occurs when the eccentricity of the line of action of the force, *F*, with respect to center of the plate is infinity ($e.\cos(\gamma) = \infty$). The rate of energy dissipated along an arbitrary element of *dx* by *dy* on top or bottom surfaces of the anchor plate with center at (*x*, *y*) and distance of $R(x,y) = \sqrt{\left(x - x_0\right)^2 + \left(y - y_0\right)^2 + (t/2)^2}$ from the center of rotation (Fig. 2(a)), is $d\dot{D}_s = \alpha s_u R(x,y)\dot{\beta}dxdy$ which can be integrated over the plate area (see Appendix A). The undrained shear strength, s_u, along top and bottom plate surfaces is assumed to be fully developed in Yang et al. (2010) formulation. The adhesion factor (α) for fully bonded plate and soil is assumed to be unity. The second dissipation term ($\dot{D}_e$) due to the resistance of the soil on the four ends of the plate could be resolved into sliding (F_{st}) and normal (F_{nt}) components (Fig. 2(b)). As these terms are dependent on the plate thickness, they vanish for infinitely thin plates. Yang et al. (2010) assumes that both the normal (F_{nt}) and sliding (F_{st}) soil resistances on plate ends are fully mobilized at failure. Thus, no interaction is assumed between normal and tangential forces along the plate edges.

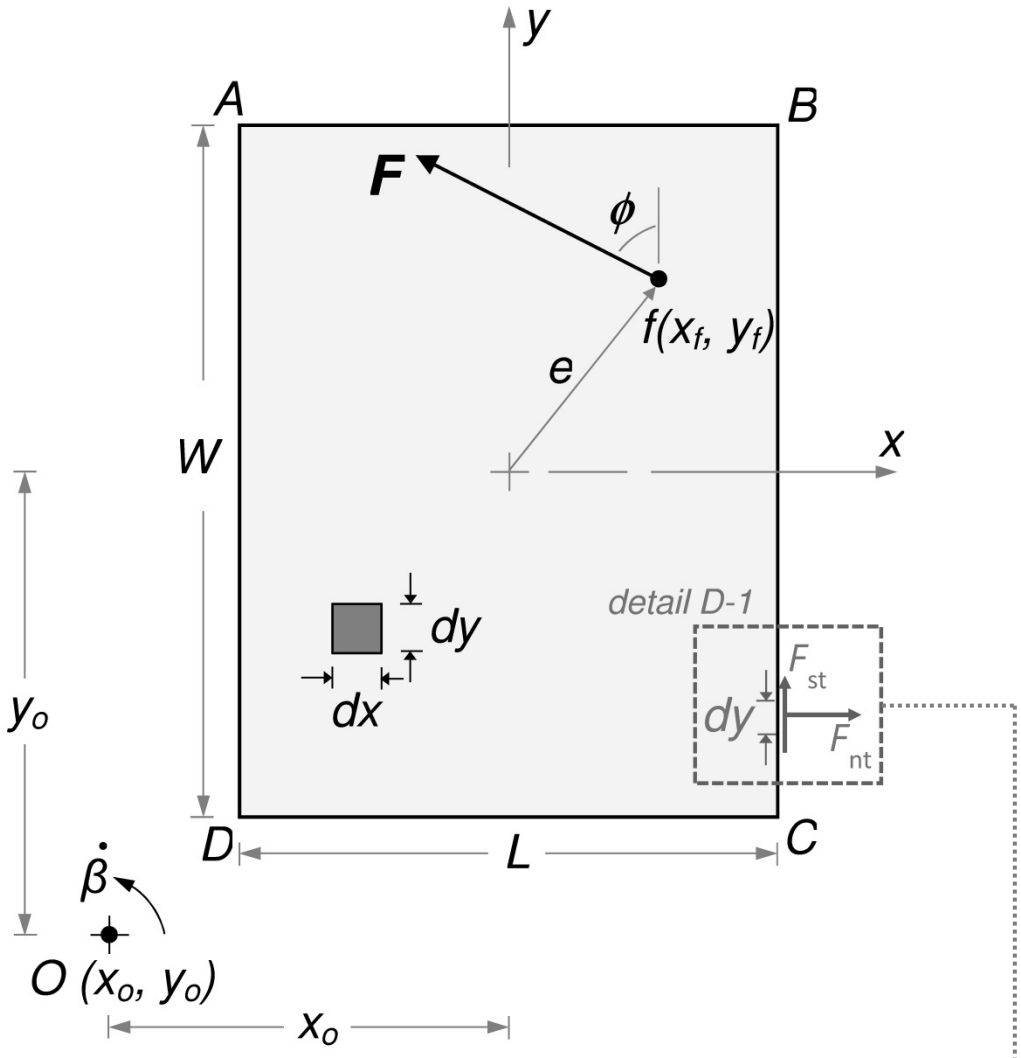

(a)

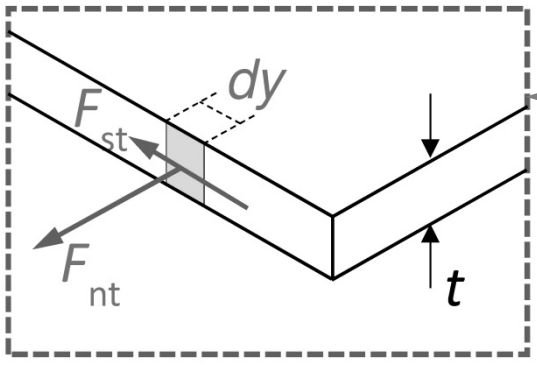

(b)

Figure 2- Upper bound PLA mechanism for shear-torsion loading of a plate anchor: (a) plan view of the plate and mechanism; (b) Detail D-1: isometric view of the plate edge and acting normal (F_{nt}) and tangential (F_{st}) forces

Assuming an arbitrary element of t (plate thickness) by dl (= dx and dy for edges parallel to x and y axis respectively) on each edges of the plate (Fig. 2), the sliding and normal components are calculated (i.e. $dF_{st} = \alpha.s_u.t.dl$ and $dF_{nt} = N_e.s_u.t.dl$). N_e is a simple plane strain bearing capacity factor for each element to determine the normal component and is assumed equal to N_e=7.5 (O'Neill et al. 2003). The adhesion factor (α) of unity is also adopted for fully attached plate and soil. Total values of normal and tangential portions of soil resistance on the plate edges are determined by integrating along each plate edge (see Appendix A).

By substituting the dissipation terms in Eq. 1 and canceling out the angular velocity, $\dot{\beta}$, an expression is obtained in terms of x_o and y_o for external force, F. A least upper bound is obtained by minimizing F with respect to the rotation coordinates (x_o, y_o).

Issues with the existing Yang et al. (2010) PLA Solution

Tables 1 and 2 summarize the results of the Yang et al. (2010) PLA solutions as well as the 3D-FE developed by Nouri (2013) for the ultimate shear and torsion bearing capacity of the square and rectangular (W/L = 2) plates of various thicknesses (t/L = 0, 1/20, 1/14, 1/10, and 1/7). The Yang et al. (2010) PLA solution developed by Yang et al. (2010) seem to reasonably predict the ultimate shear bearing capacity ($N_{s,max}$) regarding its satisfactory agreement with the 3D-FE results for plate of different geometry. However, the unconservative over-prediction of the 3D-FE results for maximum torsional resistance ($N_{t,max}$) by the PLA solution and the growing difference for the thicker plates suggest the inaccuracy of the current PLA formulation to predict torsional resistance for plates of larger thickness.

Fig. 3 plots present the PLA and 3D-FE derived normalized shear-torsion interaction curve for rectangular (W/L=2) plates. Comparison of $H_x/H_{x,max}$ - T/T_{max} yield envelopes in Fig. 3(a) indicates the unconservative tendency of the PLA approach to over-predict the bearing capacity

by 20-30%. The over-prediction trend is also repeated in PLA derived $H_y/H_{y,max}$ - T/T_{max} interaction curves for rectangular and square plates (Figs. 3(b) and 4, respectively). PLA envelopes show a vertical non-interacting portion for low values of torsional resistance (T/T_{max}<0.3-0.4), which is not observed in 3D-FE envelopes. This vertical section indicates that the PLA approach predicts no change of the shear resistance by the plate torsion which ends in overestimating the bearing capacity values. This non-interacting vertical portion in the PLA envelopes shortens for the plates of smaller thickness and eventually vanishes for infinitely thin plate (t =0), since the resistance for thinner plates is solely controlled by the energy dissipated on the top and bottom surfaces of the plate. This could also confirm the inaccuracy of simplifying assumption on full mobilization of shear and normal forces acting on the edges of the plate.

Fig. 5 also presents PLA and 3D-FE normalized interaction curves for anchor plate under two-way in-plane translation ($H_x/H_{x,max}$ - $H_y/H_{y,max}$) for square and rectangular (W/L = 2) plates with thicknesses of t = L/20 and L/7. PLA unconservative tendency to over-estimate the shear bearing capacity is repeated similar to shear-torsion yield envelops. The non-interacting segment appears again at both ends of the yield envelope where maximum shear resistance is expected to diminish due to the shear resistance mobilization in another perpendicular direction according to 3D-FE results. This unconservative trend is more pronounced for plate anchors of smaller aspect ratio and higher thicknesses, as the yield envelope for rectangular plate of t = L/20 nearly tracks 3D-FE data points.

Approaching the results of Yang et al. (2010) PLA and 3D-FE yield envelopes and ultimate torsional resistance for smaller thicknesses suggests that Yang's assumption on the negligible interaction of sliding (F_{st}) and normal (F_{nt}) forces on the edges of the plate at soil failure condition is not accurate for plates of finite thickness as also suggested by Yang et al. (2010).

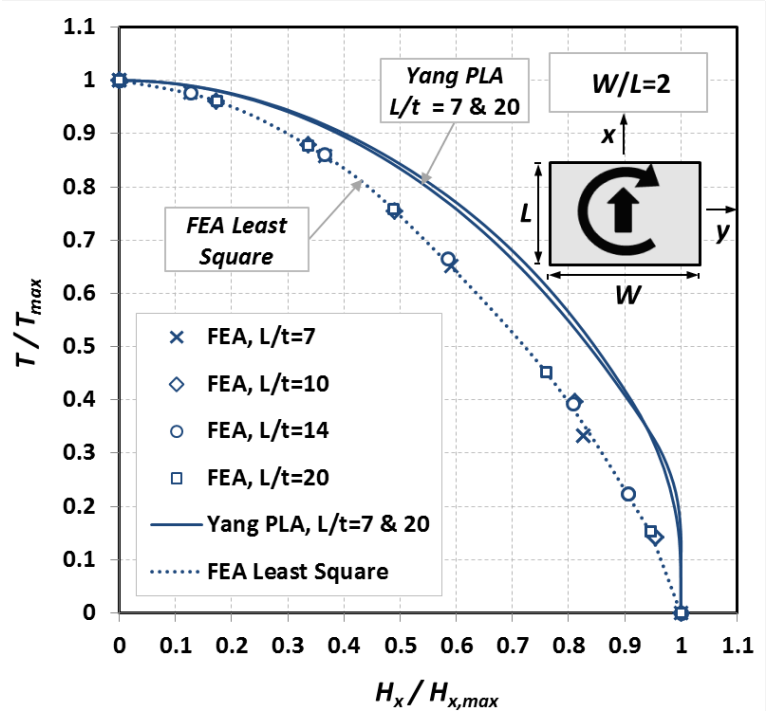

(a)

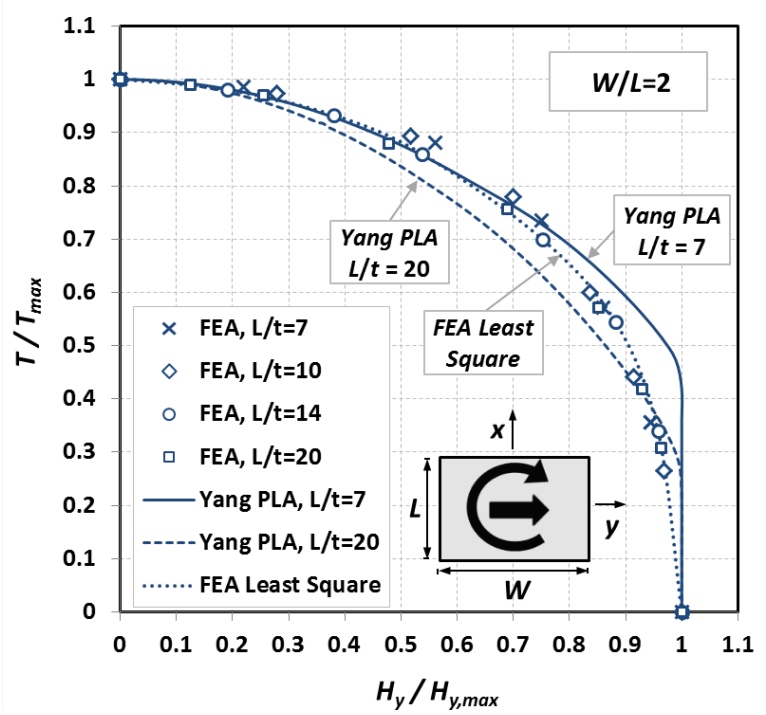

(b)

Figure 3- Comparison of Yang et al. (2010) PLA and 3D-FE predictions for rectangular (*W*/*L*=2) plates under combined: (a) shear*x*-torsion; (b) shear*y*-torsion

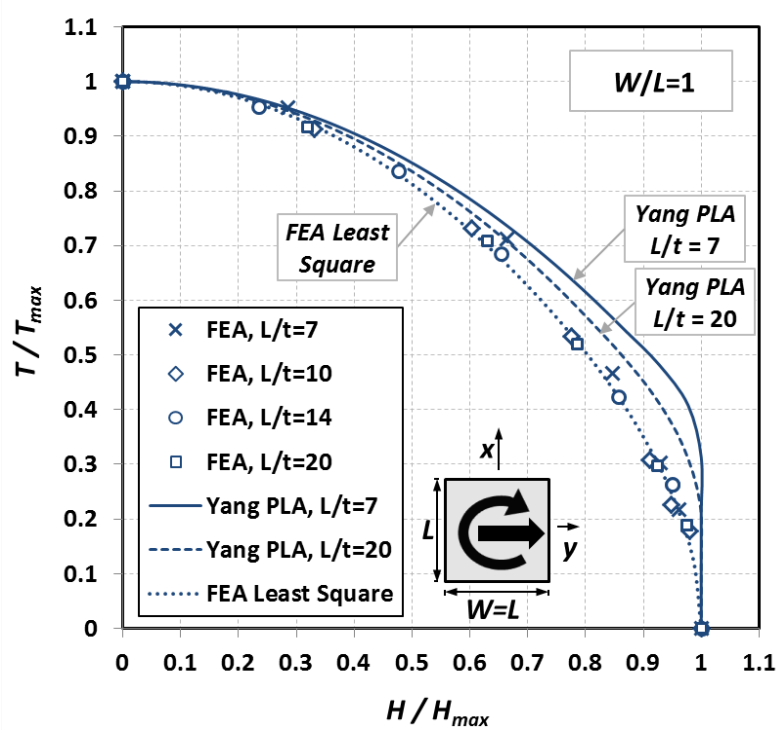

Figure 4- Comparisons of the Yang et al. (2010) PLA and 3D-FE predictions for square (W/L=1) plate under combined shear-torsion

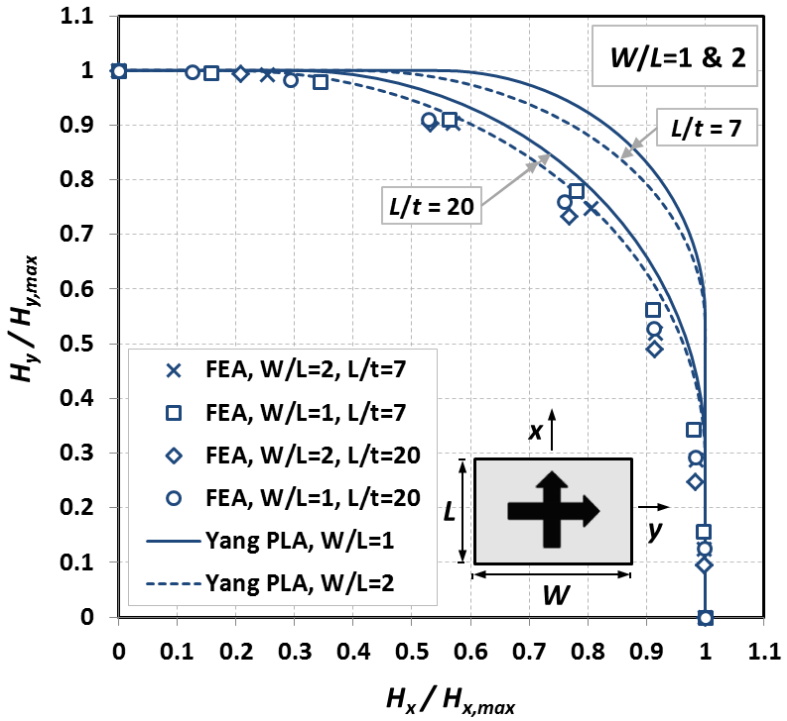

Figure 5- Comparisons of the Yang et al. (2010) PLA and 3D-FE predictions for square and rectangular (W/L=2) plates under coplanar shear$x$ - shear$y$

As shown in Tables 1 and 2, this assumption could be valid for plates subjected to one-way pure translation where the edges are under pure normal or shear forces, but when the plate is subjected to torsion or combined two-way in-plane translation, there will be a combination of shear and normal reaction forces acting on the plate edges. Neglecting the interaction and assuming full mobilization of both sliding and normal components may result in estimating higher dissipated energy due to soil sliding and normal resistance on the plate edges and over-predicting the overall plate resistance especially for thicker plates. Thus, the insensitivity of 3D-FE derived yield surfaces to plate thickness (see Figs. 3, 4, and 5) is not predicted by the current upper bound solution. Modification of the assumption for interaction of sliding-normal forces on the plate edges could be incorporated in the existing PLA solution to improve the current formulation. The modified PLA solution will be proposed in the following sections of this study.

Table 1. Comparison of PLA and FE results for the ultimate shear force ($N_{s,max}$) and torsion moment ($N_{t,max}$) bearing capacity factors for square plate

Mode of Plate Loading	Plate thickness (t/L)	Finite Element Values	Upper Bound Solution		Difference of FE and Yang et al. (2010) (%)	Difference of FE and Current study (%)
			Yang et al. (2010)	Current (modified)		
Shear, $N_{s,max}$	0	2	2	2	0.0	
	1/20	2.90	2.85	2.85	-1.7	
	1/14	3.30	3.21	3.21	-2.7	
	1/10	3.67	3.70	3.70	0.8	
	1/7	4.37	4.43	4.43	1.4	
Torsion, $N_{t,max}$	0	0.765	0.76	0.76	-0.7	-0.7
	1/20	1.14	1.24	1.16	8.8	1.8
	1/14	1.26	1.44	1.34	14.3	6.3
	1/10	1.34	1.71	1.57	27.6	17.2
	1/7	1.47	2.12	1.90	44.2	29.3

Table 2. Comparison of PLA and FE results for the ultimate shear force ($N_{sx,max}$, $N_{sy,max}$) and torsion moment ($N_{t,max}$) bearing capacity factors for rectangular plate (W/L=2)

Mode of Plate Loading	Plate thickness (t/L)	Finite Element Values	Upper Bound Solution		Difference of FE and Yang et al. (2010) (%)	Difference of FE and Current study
			Yang et al. (2010)	Current (modified)		
Shear, $N_{sx,max}$	0	2	2	2	0.0	
	1/20	2.84	2.80	2.80	-1.4	
	1/14	3.21	3.14	3.14	-2.2	
	1/10	3.55	3.60	3.60	1.4	
	1/7	4.20	4.29	4.29	2.1	
Shear, $N_{sy,max}$	0	2	2	2	0.0	
	1/20	2.50	2.48	2.48	-0.8	
	1/14	2.72	2.68	2.68	-1.5	
	1/10	2.93	2.95	2.95	0.7	
	1/7	3.32	3.36	3.36	1.2	
Torsion, $N_{t,max}$	0	1.19	1.19	1.19	0.0	0.0
	1/20	1.66	1.75	1.67	5.4	0.6
	1/14	1.84	2	1.89	8.7	2.7
	1/10	1.98	2.32	2.18	17.2	10.1
	1/7	2.27	2.81	2.59	23.8	14.1

ANALYTICAL BASELINE SOLUTIONS

This study also introduces a number of convenient analytical and semi-analytical solutions which can provide useful reference solutions to evaluate the modified PLA and FEA approaches.

Pure Sliding and Rotation: Limit Equilibrium Approach

Nouri et al. (2014) proposed a limit equilibrium (LE) approach to estimate the pure sliding and torsional resistance for shallow foundations. This study uses the same general LE methodology and failure mechanism to derive bearing capacity factors for pure sliding in the x and y directions for a deeply embedded plate anchor of thickness t, in a homogeneous soil with an adhesion factor α at the soil-plate interface. Following expressions are developed to calculate bearing capacity

from the assumed stress distribution and failure mechanism in Fig. 6:

$$N_{sx,max} = \frac{H_{x\max}}{s_u LW} = 2\alpha + 2\left[\alpha \frac{L}{W} + N_e\right]\frac{t}{L} \quad (2)$$

$$N_{sy,max} = \frac{H_{y\max}}{s_u LW} = 2\alpha + 2\left[\alpha + N_e \frac{L}{W}\right]\frac{t}{L} \quad (3)$$

where s_u is the soil undrained shear strength, L and W are the smaller and larger sides of the plate, and N_e is the simple plane strain bearing capacity factor equal to 7.5 (O'Neill et al. 2003). The adhesion factor, α, for the fully bonded condition is assumed equal to unity. Note that the results of two and three dimensional sliding resistance are typically normalized by $s_u L$ and $s_u WL$ respectively. The above expression for pure x-shear capacity factor, $N_{sx,max}$, for a strip plate ($L/W \approx 0$) reduces to $N_{s,max}=2(1+N_e.t/L)$ as proposed by O'Neill et al. (2003) for ultimate parallel plate capacity in 2D plane strain condition.

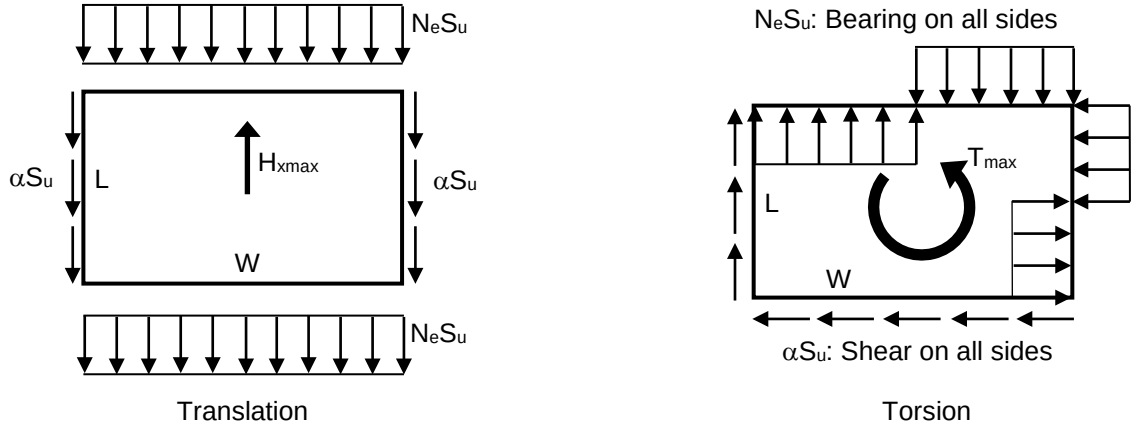

Figure 6- Assumed stress distribution of plate pure sliding and torsion for limit equilibrium solution

The plate aspect ratio (W/L) does not influence the pure shear capacity of the plate anchor under x-sliding, where N_{sx} (Eq. 2) yields to 4.29 and 4.15 for rectangular (W/L=2) and plane strain strip plate (W/L = 20) of $t = L/7$ (about 3% different). Evidently, this difference becomes even less for plates of smaller thickness, where in the extreme condition the N_{sx} becomes independent of W/L

for infinitely thin plate (N_{sx} =2 for square and rectangular plates).

For the special case of pure torsion with zero thickness, t = 0, the following LE solution provides a convenient benchmark for ultimate torsional resistance T_{max0} (the subscript '0' referring to zero thickness) to compare with the numerical calculations:

$$T_{max0} = 2s_u \int_{-W/2}^{W/2} \int_{-L/2}^{L/2} \sqrt{x^2 + y^2}\, dxdy \tag{4}$$

Results of the above LE based solution for pure torsion also conforms with Yang et al. (2010) PLA approach where they propose the following closed form solution:

$$N_{t\max 0} = T_{max0} / (s_u WL^2) = \frac{\alpha (W/L)^2}{6}\left\{\frac{\sin\theta_o}{\cos^2\theta_o} + ln\left[\tan\left(\frac{\pi}{4}+\frac{\theta_o}{2}\right)\right]\right\} + \alpha\frac{L/W}{6}\left\{\frac{\cos\theta_o}{\sin^2\theta_o} - ln\left[\tan\left(\frac{\theta_o}{2}\right)\right]\right\} \tag{5}$$

where $\theta_o = \tan^{-1}(L/W)$. Note that the results of two and three dimensional moment resistance are typically normalized by $s_u L^2$ and $s_u WL^2$ respectively.

For the general case of a plate with finite thickness, we used a limit equilibrium based approach by summing the torsion resistance on the edges of a rotating plate (Fig. 6). We adopted the simplifying assumption of no interaction effects between bearing (normal) and tangential resistance acting on the plate edges (i.e. full mobilization of these components as shown in Fig. 6) which yielded the following expression for additional torsional resistance from plate edges:

$$\Delta N_{t\max e} = C_f \left[\frac{1}{2} N_e \left(\frac{W}{L} + \frac{L}{W}\right) + 2\alpha\right]\frac{t}{L} \tag{6}$$

A correction factor, C_f, is included in Eq. 6 to emphasize that some adjustment for interaction effects on plate edges is needed. The total torsional resistance is the sum of Eqs 5 and 6, N_{tmax0} + ΔN_{tmaxe}. This closed-form expression portrays the variables affecting torsional capacity and, as will be seen, offers a simple calibration expression to match the finite element solutions.

Combined loading

For plate of zero thickness ($t/L = 0$) an upper bound virtual work analysis provides a useful check for the Yang et al. (2010) PLA and FEA. Nouri et al. (2014) originally introduced this approach to evaluate the resistance of surface foundations (i.e. embedment of zero) under one-way eccentric parallel loading [Fig. 7(b)]. This study generalizes the same approach for a plate of zero thickness subjected to an eccentric translational loading [Fig. 7(a)]: A horizontal load H is applied at a distance $eCos(\gamma)$ from the center of the plate, with an eccentricity angle of ψ, load angle of γ, and an associated motion about a center of rotation located a distance ρ from the center. Equating external virtual work, $\dot{W}$, to internal energy dissipation leads to:

$$H = \frac{\dot{D}}{(\rho + eCos\gamma)\dot{\beta}} \tag{7}$$

where $\dot{\beta}$ is a virtual angular velocity. This relationship is written based on the assumption that the line perpendicular to external force, H, through center of rotation is passing through the center of the plate. This assumption has been proved to be valid for infinitely thin plate ($t/L = 0$) through PLA parametric analysis. The validity of this assumption could also be evaluated through assuming the center of rotation in a random location and developing the formulation. However, taking advantage of the PLA proved assumption will keep the solution simple which is the main purpose of developing the baseline formulation.

The rate of internal energy dissipation $\dot{D}$ is the soil resistance times the local velocity integrated over the plate area:

$$\dot{D} = 2s_u \dot{\beta} \int_{-W/2}^{W/2} \int_{-L/2}^{L/2} \sqrt{\left[x + \rho Cos(\psi + \gamma)\right]^2 + \left[y + \rho Sin(\psi + \gamma)\right]^2}\, dxdy \tag{8}$$

A least upper bound collapse load is obtained by minimizing H in Eq. 7 with respect to ρ and setting it equal to zero, with the assumption of constant e, ψ, and γ values, which leads to:

$$H = \frac{1}{\dot{\beta}} \frac{\partial \dot{D}}{\partial \rho} \tag{9}$$

For the case of zero plate thickness the collapse load then becomes equal to:

$$H = 2s_u \int_{-W/2}^{W/2} \int_{-L/2}^{L/2} \frac{\rho_{opt} + xCos(\psi+\gamma) + ySin(\psi+\gamma)}{\sqrt{\left[x + \rho_{opt} Cos(\psi+\gamma)\right]^2 + \left[y + \rho_{opt} Sin(\psi+\gamma)\right]^2}} dxdy \tag{10}$$

where ρ_{opt} is the distance to the optimal center of rotation corresponding to a least upper bound. For any arbitrary value of ρ_{opt}, $\dot{D}$ and H could be derived through numerical evaluation of integrals in Eqs. 8 and 10. The eccentricity, e, corresponding to the arbitrary value of ρ_{opt}, is obtained from Eq. 7 with known $\dot{D}$, H, and ρ_{opt}. Parametric study is also possible with evaluating the equations for a sweep of ρ_{opt} values.

For a special case of eccentricity and loading directions aligned with either the major or minor axis [e.g. eccentricity angle of ψ=0.0° and γ=0.0° as shown in Fig. 7(b)] Eqs. 7, 8, and 10 could be reduced to a more concise form (Nouri et al. 2014):

$$H = \frac{\dot{D}}{(\rho + e)\dot{\beta}} \tag{11}$$

$$\dot{D} = 2s_u \dot{\beta} \int_{-W/2}^{W/2} \int_{-L/2}^{L/2} \sqrt{(\rho + x)^2 + y^2}\, dxdy \tag{12}$$

$$H = 2s_u \int_{-W/2}^{W/2} \int_{-L/2}^{L/2} \frac{\rho_{opt} + x}{\sqrt{(\rho_{opt} + x)^2 + y^2}} dxdy \tag{13}$$

Although the analytical evaluation of the double integral in Eq. 12 to calculate $\dot{D}$ generates a long expression, this equation could be reduced to a single integral (Appendix B) appropriate for the simple design spreadsheet calculations. In addition, analytical integration of Eq. 13 results in a closed-form expression for H:

$$
\begin{aligned}
H &= 2s_u\left[a_1^2\ln\left|\frac{b_1+W/2}{b_1-W/2}\right| - a_2^2\ln\left|\frac{b_2+W/2}{b_2-W/2}\right| + W(b_1-b_2)\right] \\
a_1 &= \rho_{opt} + L/2 \\
a_2 &= \rho_{opt} - L/2 \\
b_1 &= \sqrt{a_1^2 + W^2/4} \\
b_2 &= \sqrt{a_2^2 + W^2/4}
\end{aligned}
\tag{14}
$$

Contrary to the PLA approach, the proposed method requires no search or optimization procedure since the final solution directly relates the eccentricity, *e*, to the distance to the optimal center of rotation, ρ_{opt}, and thus the equivalent external force $H=H(\rho_{opt})$ (Eq.14). This feature also eliminates the complications in optimization procedure in locating the absolute minimum which could be mistaken by the greater local minimums. Regardless of the numerical integration required to evaluate the rate of energy dissipation, the final solution in this method is derived through closed-form expressions easy to implement in spreadsheets. Thus, it can provide a simple robust tool for routine design calculations.

Conducting the analysis for a sweep of ρ values generates a predicted reduction in load capacity (H/H_{max}) versus eccentricity *e* for a plate under planar eccentric load aligned with the major or minor plate axis. As shown in Fig. 8, shear resistance for loading in the *x* and *y* directions show a significant reduction. Square plates, $W/L = 1$, experience the greatest decrease in *H* resistance, with eccentricity as low as $e/L = 0.1$ reducing load capacity by more than 5% and eccentricity $e/L = 0.5$ (load application at the edge of the plate) reducing capacity by more than 40%. With increasing aspect ratio *W*/*L* the plate anchor becomes progressively more resistant to eccentric loading. The predictions also show that the reduction in capacity is always the greatest for loading in the *x* direction; i.e., for load orientations normal to the long axis of the plate. Note that torsion is equal to $T=H.\,eCos(\gamma)$. Results of this formulation will be referred as $PLA_{t=0}$, hereafter.

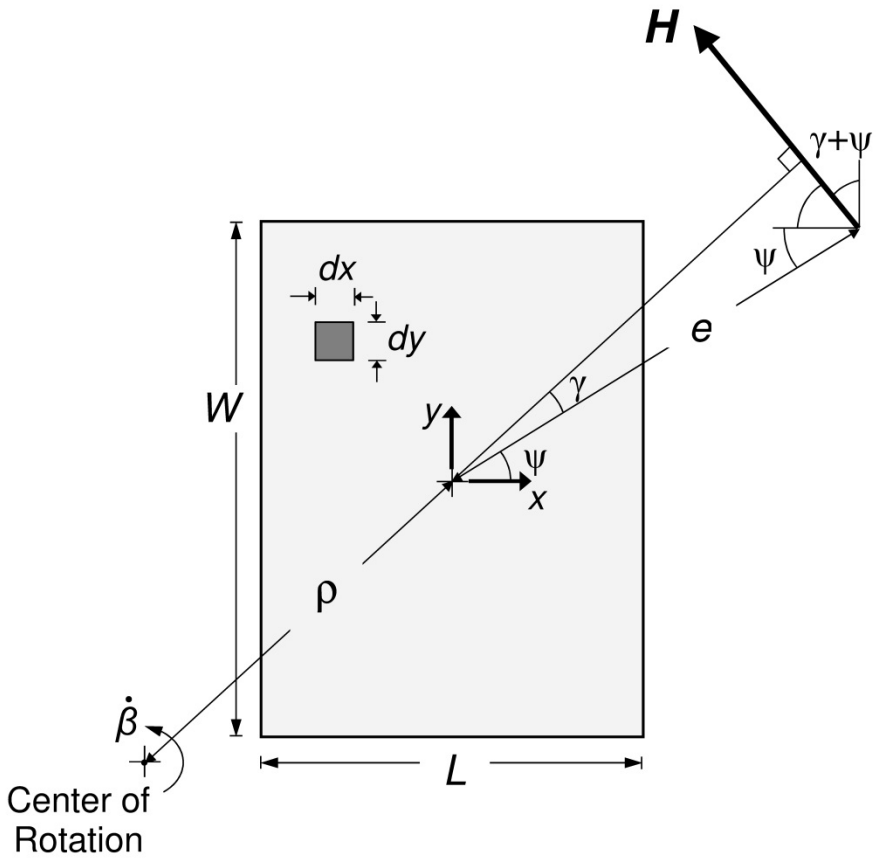

(a)

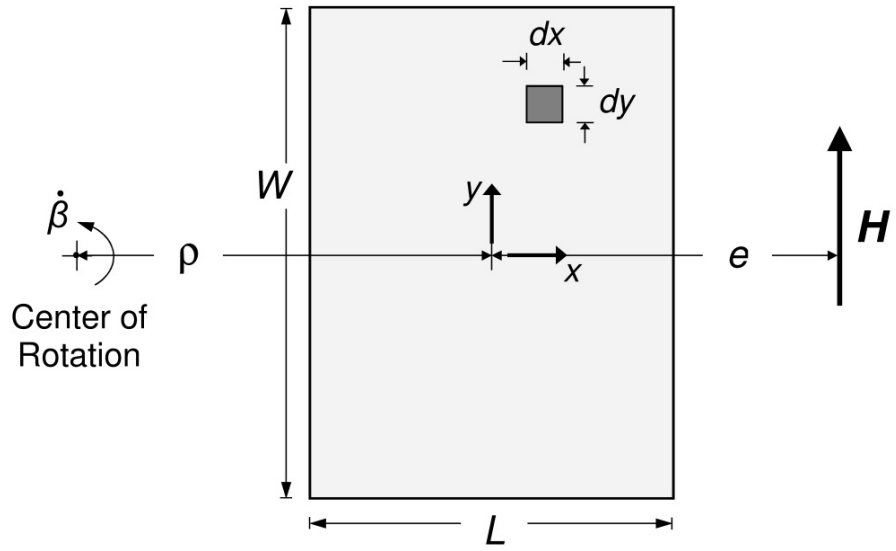

(b)

Figure 7- Model for virtual work analysis for combined sliding-torsion: (a) generalized condition; (b) eccentricity and loading directions aligned with the axis

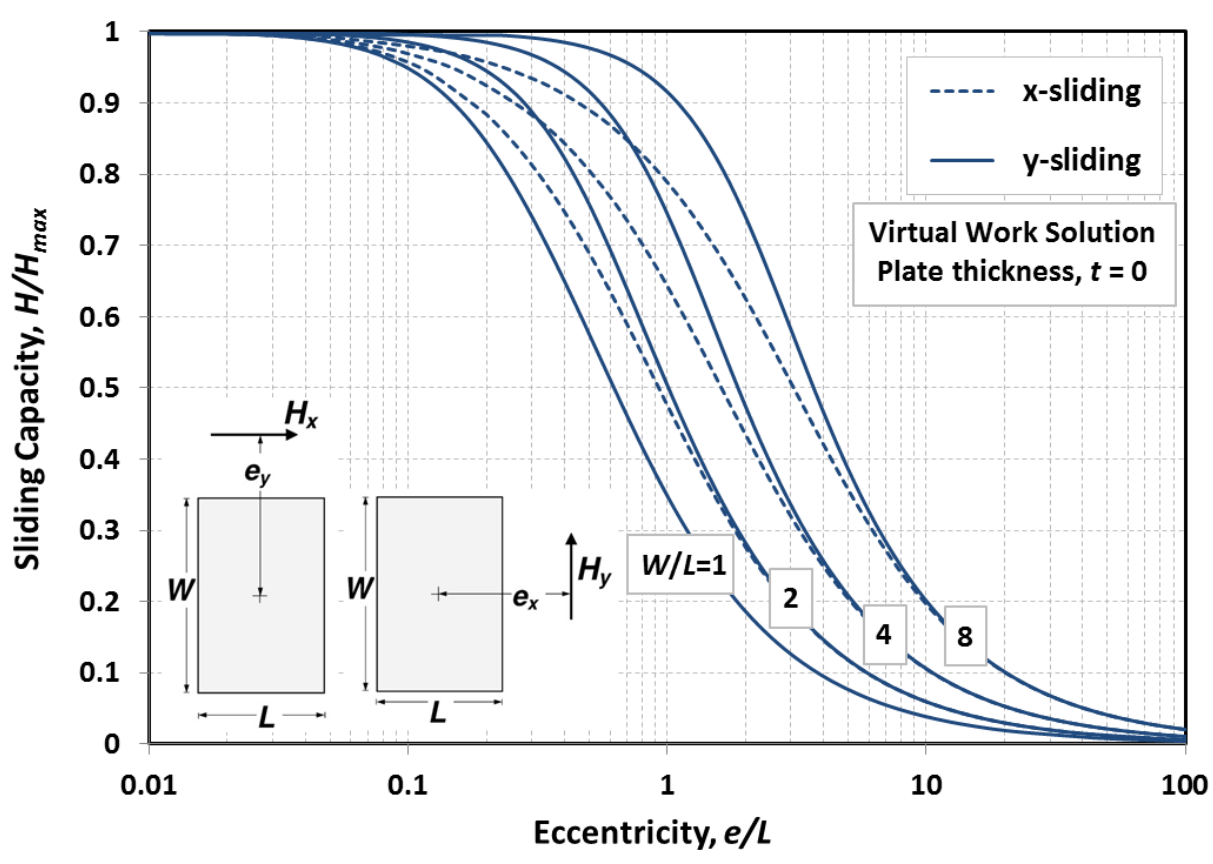

Figure 8- Reduction of shear capacity with eccentricity for square and rectangular plates of zero thickness

Modified PLA solution

To improve the Yang et al. (2010) PLA formulation and incorporate the shear-normal force interaction along the edges of the plate, the dissipation term that accounts for the soil resistance along the plate edges, $\dot{D}_e$, should be revised. Other terms of dissipation (i.e. energy dissipation along the top and bottom surfaces of the plate, $\dot{D}_s$) and external work remains unchanged in the revised formulation.

The assumed angular velocity, $\dot{\beta}$, of the plate rotating about point O(x_o, y_o) in Fig. 2, prescribes the relative increments of displacement in the normal and parallel directions with respect to the plate edges as follows (based on the assumption of rigid plate):

For AB and CD (sides parallel to x axis): $\begin{cases} \dot{u}_n = |x - x_0|\dot{\beta} \\ \dot{u}_s = |y - y_0|\dot{\beta} \end{cases}$ (15-a)

For AD and BC (sides parallel to y axis): $\begin{cases} \dot{u}_n = |y - y_0|\dot{\beta} \\ \dot{u}_s = |x - x_0|\dot{\beta} \end{cases}$ (15-b)

where $\dot{u}_n$ and $\dot{u}_s$ are displacement increments normal and parallel to the plate vertical end faces, respectively. A general relationship for the sliding-normal interaction curve, f (N_{nt}, N_{st}), is adopted as follows:

$$f(N_{nt}, N_{st}) = \left(\frac{N_{nt}}{N_{nt,\max}}\right)^m + \left(\frac{N_{st}}{N_{st,\max}}\right)^n - 1 = 0 \quad (16)$$

where $N_{nt} = F_{nt}/(s_u \times t \times dl)$ and $N_{st} = F_{st}/(s_u \times t \times dl)$ are non-dimensional forms of F_{nt} and F_{st} (respectively normal and shear forces on the plate edges in Fig. 2) acting on arbitrary element of dimensions t (plate thickness) by dl (= dx and dy for sides parallel to x and y axis respectively) on the plate edges as shown in Fig. 2. $N_{nt,max} = N_e$ which is the plane strain bearing capacity factor, is typically equal to 7.5 (O'Neill et al. 2003). The maximum sliding force $N_{st,max}$ is equal to adhesion factor α and assumed to be unity for the plate fully bonded to the soil. The assumption of no detachment is necessary for deriving a limit analysis solution with an associated flow rule, but the adhesion factor could take any value between zero and unity. Here the assumption of α=1 is consistent with the fully bonded condition. The center of area of the element on the edge of the plate with coordinates (x,y) is assumed to be the representative point of the element. As discussed by Prager (1959) the loads and plastic displacements associated with yielding of the foundation are treated as generalized plastic strains. As the upper bound solution is obtained for failure conditions, this study assumes that the increments of elastic displacement are negligible when compared to the plastic increments. Therefore, assuming an associated flow rule, increments of total displacements of the anchor plate in directions normal and tangential to the

plate edges at point (x, y) at the failure condition could be calculated as follows:

$$\dot{u}_{nt} = \dot{u}_{nt}^{p} = \lambda \frac{\partial f(N_{nt}, N_{st})}{\partial N_{nt}} = \lambda \frac{m N_{nt}^{m-1}}{(N_{nt,\max})^{m}}$$
$$\dot{u}_{st} = \dot{u}_{st}^{p} = \lambda \frac{\partial f(N_{nt}, N_{st})}{\partial N_{st}} = \lambda \frac{n N_{st}^{n-1}}{(N_{st,\max})^{n}} \quad (17)$$

By dividing the above two expressions and substituting $\dot{u}_n$ and $\dot{u}_s$ from Eqs. (15-a) and (15-b) for each plate edge, $\dot{u}_{nt}$, $\dot{u}_{st}$, λ and $\dot{\beta}$ are eliminated and expression in terms of N_{nt} and N_{st} are obtained as follows:

For AB and CD (sides parallel to x axis):
$$\frac{|x - x_0|}{|y - y_0|} = \left(\frac{m}{n}\right)\left(\frac{N_{nt}^{m-1}}{N_{st}^{n-1}}\right)\left(\frac{N_{st,\max}^{n}}{N_{nt,\max}^{m}}\right) \quad (18\text{-a})$$

For AD and BC (sides parallel to y axis):
$$\frac{|y - y_0|}{|x - x_0|} = \left(\frac{m}{n}\right)\left(\frac{N_{nt}^{m-1}}{N_{st}^{n-1}}\right)\left(\frac{N_{st,\max}^{n}}{N_{nt,\max}^{m}}\right) \quad (18\text{-b})$$

Going through the details to implement the sliding-normal force interaction relationship in the plasticity solution indicates that in order to obtain a “closed from” of the upper bound solution, m should be equal to n (m=n). For simplicity a circular relationship for the sliding-normal interaction curve is adopted (m=n=2):

For AB and CD (sides parallel to x axis):
$$\frac{|x - x_0|}{|y - y_0|} = \left(\frac{N_{nt}}{N_{st}}\right)\left(\frac{N_{st,\max}}{N_{nt,\max}}\right)^{2} \quad (19\text{-a})$$

For AD and BC (sides parallel to y axis):
$$\frac{|y - y_0|}{|x - x_0|} = \left(\frac{N_{nt}}{N_{st}}\right)\left(\frac{N_{st,\max}}{N_{nt,\max}}\right)^{2} \quad (19\text{-b})$$

Therefore, having two equations, (19-a) or (19-b) and the yield surface, Eq. (16), the two unknowns, N_{nt} and N_{st}, could be determined:

For AB and CD (sides parallel to x axis):

$$\begin{cases} N_{st} = N_{st,\max}\left[\left(\dfrac{N_{nt,\max}}{N_{st,\max}}.\dfrac{|x-x_0|}{|y-y_0|}\right)^2+1\right]^{-0.5} \\ N_{nt} = \left(\dfrac{N_{nt,\max}}{N_{st,\max}}\right)^2\left(\dfrac{|x-x_0|}{|y-y_0|}\right)N_{st} \end{cases} \tag{20-a}$$

For AD and BC (sides parallel to y axis):

$$\begin{cases} N_{st} = N_{st,\max}\left[\left(\dfrac{N_{nt,\max}}{N_{st,\max}}.\dfrac{|y-y_0|}{|x-x_0|}\right)^2+1\right]^{-0.5} \\ N_{nt} = \left(\dfrac{N_{nt,\max}}{N_{st,\max}}\right)^2\left(\dfrac{|y-y_0|}{|x-x_0|}\right)N_{st} \end{cases} \tag{20-b}$$

296 Having N_{nt} and N_{st} in terms of element position (x, y) and point of rotation (x_0, y_0), the increment
297 of energy dissipation rate, e.g. for a representative element on BC, could be obtained as follows:

$$d\dot{D}_{e,BC} = \left(F_{st}|x-x_0| + F_{nt}|y-y_0|\right)\dot{\beta}dy = ts_u\left(N_{st}|x-x_0| + N_{nt}|y-y_0|\right)\dot{\beta}dy \tag{21}$$

298 Where x is constant for side BC of the plate, i.e. x=L/2. Therefore, the total rate of dissipated
299 energy along the BC side is calculated by integrating the above expression:

$$\dot{D}_{e,BC} = \int_{-W/2}^{W/2} d\dot{D}_{e,BC} = \int_{-W/2}^{W/2} s_u\dot{\beta}\left(N_{st}\left|\frac{L}{2}-x_0\right| + N_{nt}|y-y_0|\right)tdy \tag{22}$$

300 Following the same procedure, the rate of energy dissipation for the other edges of the plate can
301 be derived:

$$\dot{D}_{e,AB} = \int_{-L/2}^{L/2} s_u\dot{\beta}\left(N_{st}\left|\frac{W}{2}-y_0\right| + N_{nt}|x-x_0|\right)tdx \tag{23-a}$$

$$\dot{D}_{e,CD} = \int_{-L/2}^{L/2} s_u\dot{\beta}\left(N_{st}\left|\frac{W}{2}+y_0\right| + N_{nt}|x-x_0|\right)tdx \tag{23-b}$$

$$\dot{D}_{e,AD} = \int_{-W/2}^{W/2} s_u\dot{\beta}\left(N_{st}\left|\frac{L}{2}+x_0\right| + N_{nt}|y-y_0|\right)tdy \tag{23-c}$$

302 Where N_{st} and N_{nt} are substituted from Eqs. (20-a) and (20-b). Thus, the rate of energy

dissipation due to soil resistance on the plate edges is determined:

$$\dot{D}_e = \dot{D}_{e,AB} + \dot{D}_{e,CD} + \dot{D}_{e,BC} + \dot{D}_{e,AD} \quad (24)$$

The other terms of dissipation and external work remain unchanged in the revised formulation. The basis of the Yang and modified PLA solutions are summarized in Appendix A.

COMPARISON TO BASELINE AND PLA SOLUTIONS

The finite element studies are now compared to the baseline and PLA solutions through comparing the two basic components defining the yield envelope:

1- The "size" of the yield envelope quantified by the predicted maximum resistance under pure translational ($H_{x,max}$, $H_{y,max}$) and rotational (T_{max}) loading.

2- The "shape" of the yield envelope defined by the mathematical model $f\,(H_x/H_{x,max}, H_y/H_{y,max}, T/T_{max}) = 0$ which is curve fitted to the yield surface, and represented by interaction factors (i.e. *hx*, *hy*, *h*, and *mz*):

$$f\left(\frac{H_x}{H_{x,\max}}, \frac{H_y}{H_{y,\max}}, \frac{T}{T_{\max}}\right) = \left[\left(\frac{H_x}{H_{x,\max}}\right)^{hx} + \left(\frac{H_y}{H_{y,\max}}\right)^{hy}\right]^{h} + \left(\frac{T}{T_{\max}}\right)^{mz} - 1 = 0 \quad (25)$$

The mathematical relationship in Eq. 25 represents the ellipsoid interaction or yield surface in the $H_x/H_{x,max}$ - $H_y/H_{y,max}$ - T/T_{max} normalized space.

Size of the Yield Envelope: Pure Translation and Rotation

FEA, LE, and modified PLA shear and torsional bearing capacity factors are compared in Fig. 9. The FEA maximum shear resistance, $N_{s,xmax}$ and $N_{s,ymax}$, increases linearly with increasing plate thickness, *t*, similar to predictions from LE (Eqs. 2 and 3). FEA shear bearing factors are also in good agreement with LE predictions. Although the LE solutions increasingly over-predict the FEA values with increasing plate thickness, the difference does not exceed 2.8% which occurs

for the thickest square plate (t/L= 1/7). Note that LE and PLA methods generate the same solutions for the ultimate shear capacity.

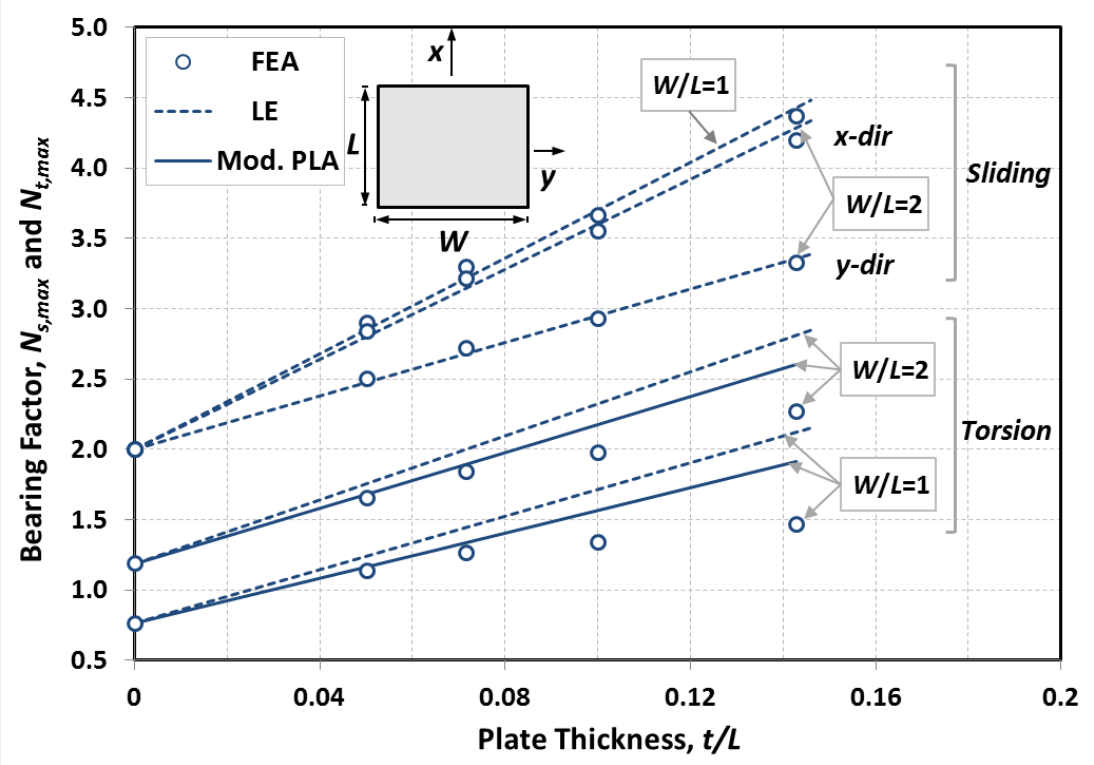

Figure 9- Normalized maximum resistance for pure translation and torsion

As for the torsional resistance, $N_{t,max}$, the FEA solution does not show a linear trend predicted by both the LE (Eqs. 5 and 6) and modified PLA formulations (Table 1 and 2; Fig. 9). With plate thickness increasing, the uncorrected (C_f = 1) LE values gradually exceed the FEA solution, by up to 44% for square plate of t/L = 1/7. It can be shown that an interaction factor C_f = 0.67 in Eq. 6 will make the limit equilibrium predictions a good fit for the finite element solutions for both the square and rectangular plates. Likewise, modified PLA tends to overestimate the increase in torsional capacity due to plate thickness. However, taking into account the interaction effect of the normal and tangential forces acting on the plate edges brings the modified PLA predictions closer to FEA values compared to Yang et al. (2010) PLA as compared in Tables 1 and 2 (e.g.

maximum difference of 29% compared to 44% for square plate of t/L = 1/7). Over-estimation of the capacity by the modified PLA with increasing thickness is also expected since the PLA formulation is based on "upper bound" limit analysis solution.

Shape of Yield Envelope: Combined Loading

Figs. 10 and 11 compare the FEA shear-torsion interaction envelopes to modified PLA and the PLA virtual work solution for infinitely thin plate (i.e. $PLA_{t=0}$, Eqs. 7-14). Load capacities are presented in normalized form, H/H_{max} versus T/T_{max}, for rectangular (Fig. 10) and square plates (Fig. 11). All the FEA predictions for the plate thickness range of $t = L/7$ to $L/20$ are essentially lying on a single curve indicating that the shape of the yield envelopes is independent of the plate thickness. A noticeable improvement is observed in modified PLA predictions for interaction response (Figs. 10 and 11) when compared with the Yang et al. (2010) PLA predictions (Figs. 3-5). Although the modified PLA values are slightly unconservative especially for thicker plates, the modified PLA predictions are generally less sensitive to the plate thickness compared to Yang et al. (2010) approach and also in overall good agreement with the FEA solutions.

The insensitivity of the FEA interaction response with respect to variations in plate thickness and close agreement to the FEA yield envelopes, introduces the $PLA_{t=0}$ solution as a realistic portrayal of the yield envelope for non-zero thickness (Fig. 11). However, except for the rectangular plate under x-shear and torsion, the $PLA_{t=0}$ predictions tend to be slightly on a conservative side.

Fig. 12 shows the modified PLA and FEA interaction diagrams for the plate under co-planar translation (i.e. non-eccentric loading with varying load directions γ). With some tendency to be on an unconservative side, especially for thicker plates, the modified PLA predictions are in good agreement with the FEA solutions. The minimal influence of the plate thickness on the

shape of FEA derived yield envelopes is better captured by the modified PLA solutions compared to the Yang PLA approach (Fig. 5). In general, the modified PLA offers markedly improved predictions compared to Yang et al. (2010) PLA (Fig. 5) for plate under co-planar shear. For the case of zero thickness, the yield envelope obtained from the $PLA_{t=0}$ solution, will be circular for both square and rectangular plates. The theoretical basis is easy to explain: for plate with area of base = A, thickness = zero, and soil undrained shear strength = s_u the sliding resistance will be constant and equal to $H_{max} = 2As_u$, regardless of the direction of sliding for Tresca yield criterion. This value actually represents the radius of the circular yield locus in the H_x -H_y space as shown in Fig. 12. This circular interaction relationship in H_x -H_y space applies for a theoretically infinitely thin plate regardless of the shape of geometric base. Fig. 12 indicates that the plate thickness induces a small but noticeable departure from a circular envelope in both PLA and FEA solutions. This departure is greater for thicker plates with lower aspect ratio and more pronounced in modified PLA predictions compared to FEA results. A simplifying assumption of a circular $H_x/H_{x,max}$ -$H_y/H_{y,max}$ yield envelope (i.e. hx=hy=2) therefore generates reasonably realistic predictions, albeit underestimating the FEA yield envelope by about 13%. Adopting interaction coefficients of hx=hy=2.5 in Eq. 25 generates a more realistic yield envelope which tracks the FEA derived solutions.

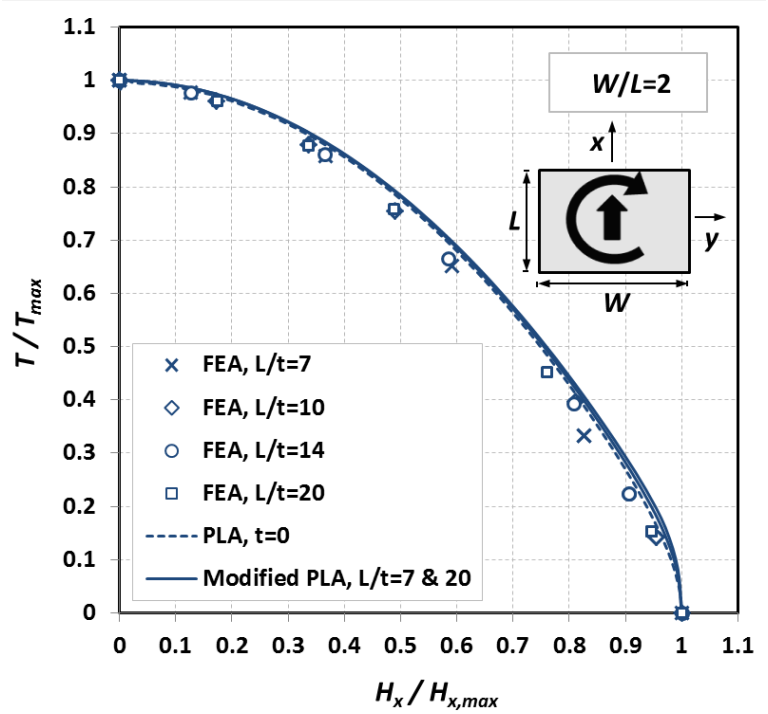

(a)

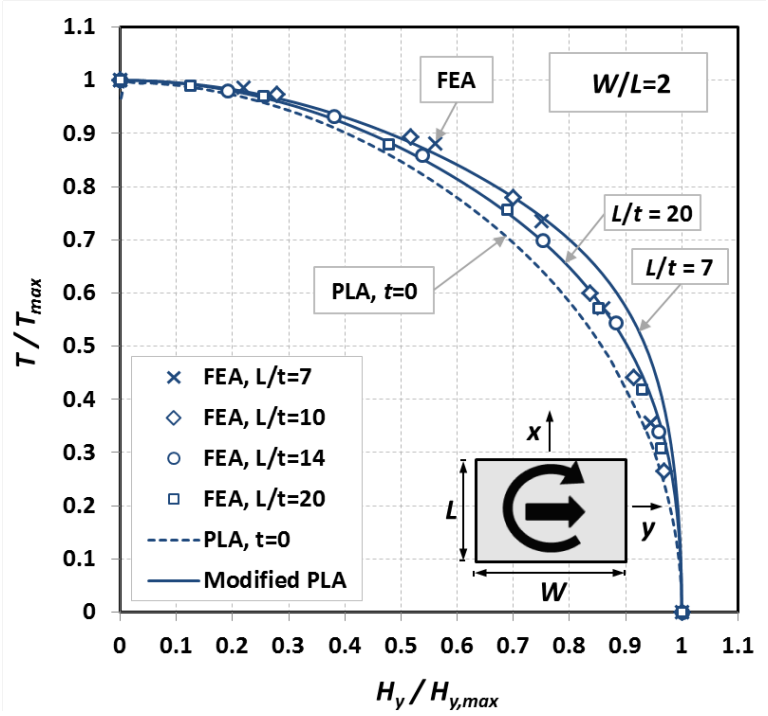

(b)

Figure 10- Analytical and FEA yield envelopes for rectangular plate: (a) shear*x*-torsion interaction; (b) sheary-torsion interaction

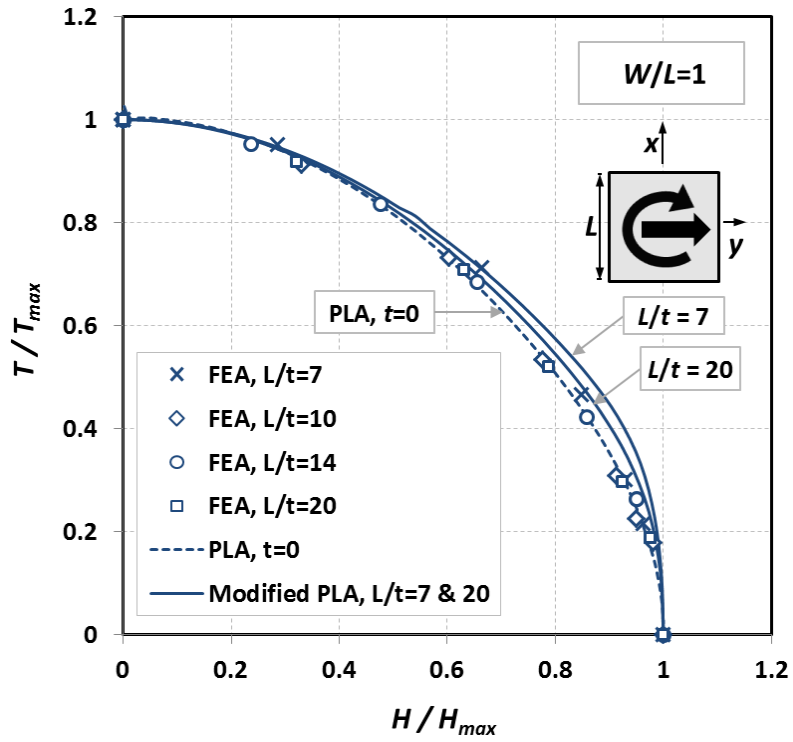

Figure 11- Analytical and FEA yield envelopes for shear-torsion interaction in square plate

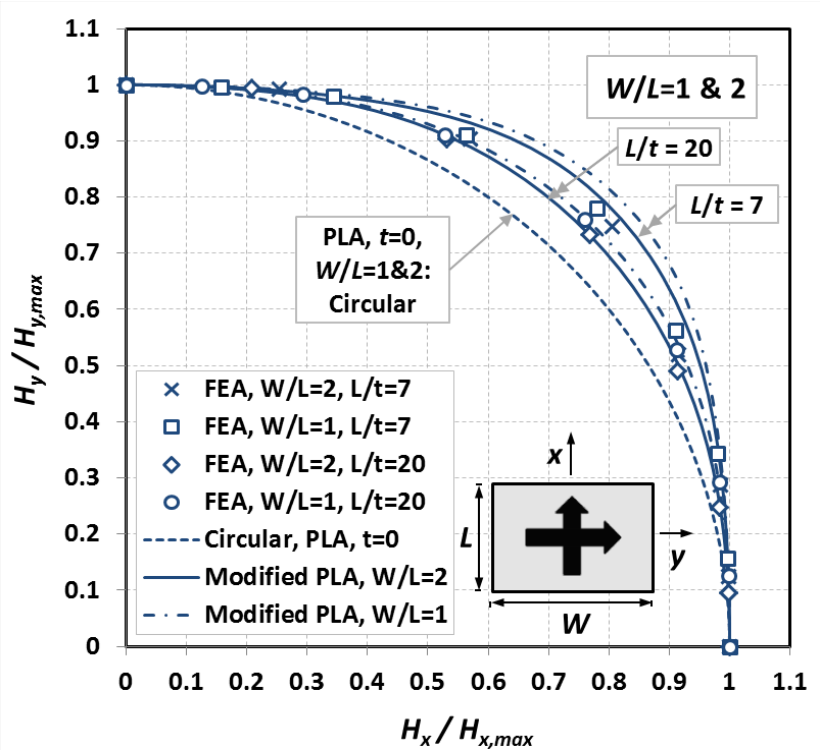

Figure 12- Analytical and FEA yield envelopes for shear*x*-shear*y*, square and rectangular plates

ECCENTRICITY AND LOAD CAPACITY REDUCTION

One-directional shear-torsion (H_x-T and H_y-T) and zero load angle (γ=0)

The reduction effect of torsion on plate sliding capacity and the combined loading effects could also be portrayed through the effect of eccentricity on the load capacity. Figs. 13-16 illustrate the sliding load reduction versus the eccentricity for square and rectangular plates of W/L = 2, 4, and 8 with thickness of $t = L/7$. Both sliding load capacity and eccentricity are expressed in dimensionless form of $N=H/s_uLW$ and e/L, respectively. The sliding load factor ($N=H/s_uLW$) is not normalized by the maximum pure capacity in Figs. 13-16, which makes the capacity reduction curves convenient to estimate both for the magnitude of shear resistance as well as the reduction/interaction effect. As discussed previously, the insensitivity of the shape of FEA sliding-torsion yield envelope and fairly accurate and simple baseline solutions to predict size and shape of the yield locus, provides the opportunity to develop a simplified approach to predict the shear-torsion plate capacity. The PLA virtual work baseline solution for zero thickness ($PLA_{t=0}$) plate under combined loading (Fig. 8) was adopted in combination with the limit equilibrium derived equations for pure translational load capacity (H_{max} using Eqs. 2 and 3 which proved to be fairly accurate), to generate the simplified solution in Figs. 13-16.

The FEA predictions for the square and rectangular (W/L=2) plates are compared with the simplified and modified PLA solutions in Figs. 13 and 14, while Figs. 15 and 16 just include the results of analytical simplified and modified PLA predictions for plates of W/L=4 and 8. Figs. 14-16 also evaluate the effect of eccentricity angle (ψ) for the rectangular plates sliding in x and y directions ($\psi = 90^\circ$ and 0° when $\gamma = 0^\circ$) with various eccentricities.

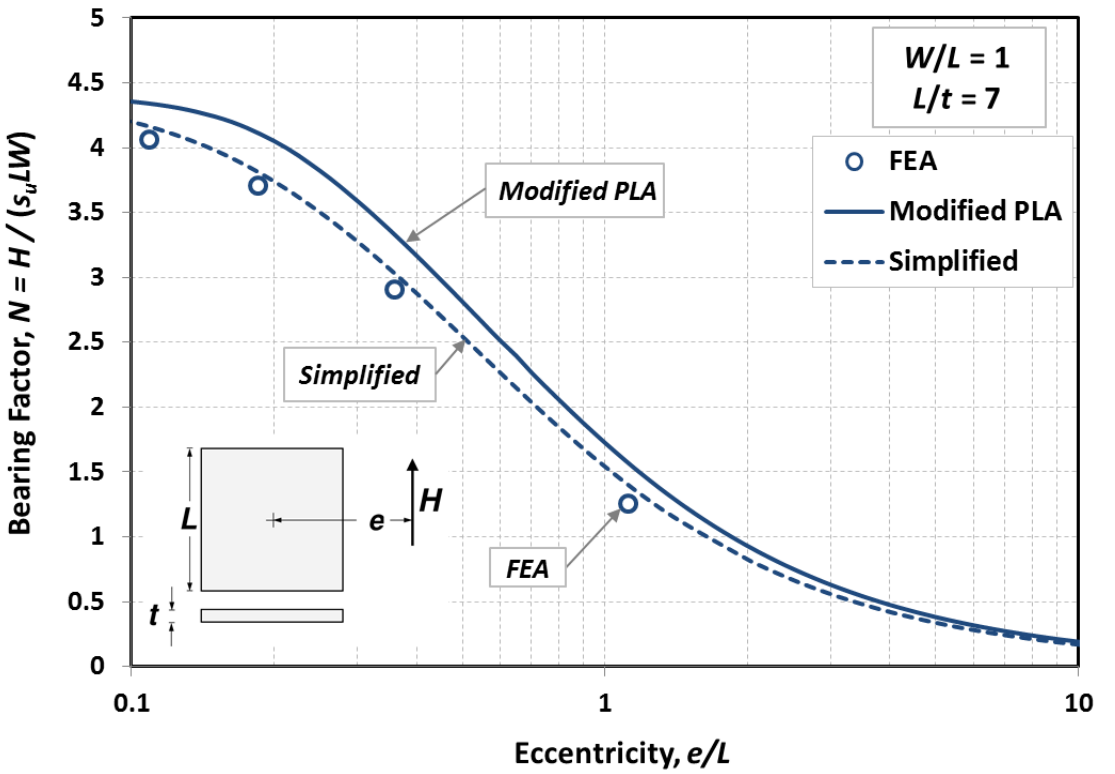

Figure 13- Reduction effect of eccentricity on sliding load capacity for square plate of $t = L/7$

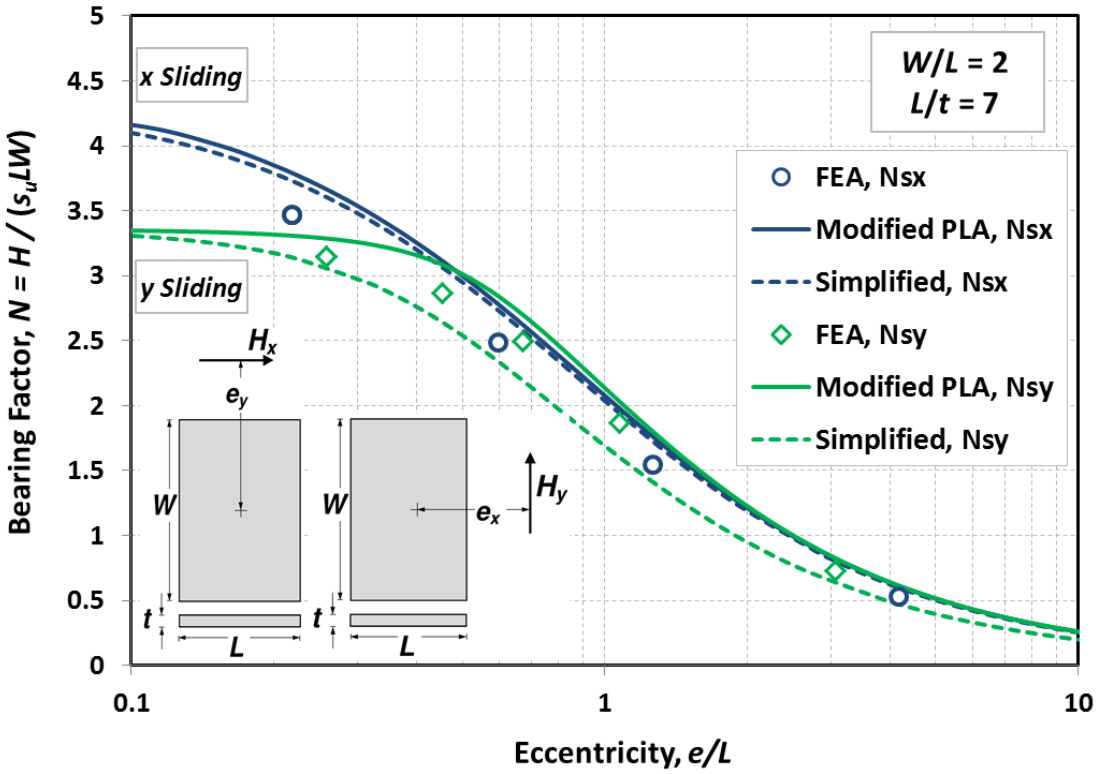

Figure 14- Reduction effect of eccentricity on sliding load capacity for rectangular (W/L=2) plate of $t = L/7$

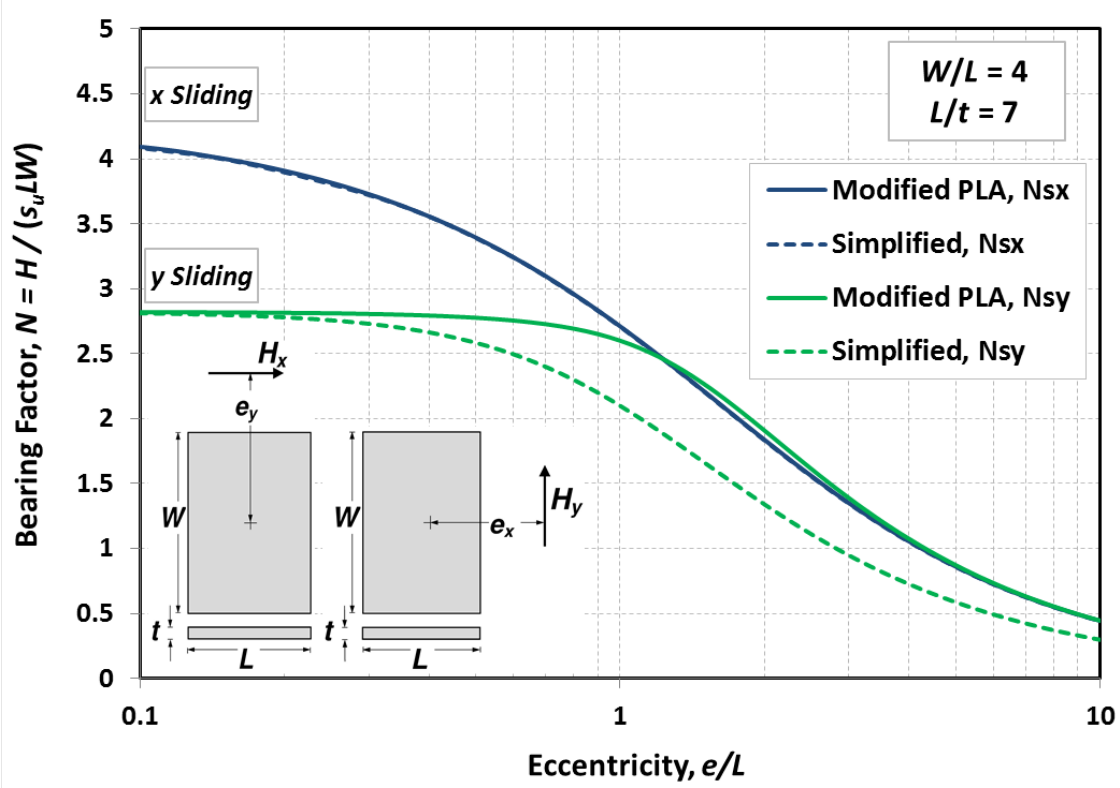

Figure 15- Reduction effect of eccentricity on sliding load capacity for rectangular (W/L=4) plate of $t = L/7$

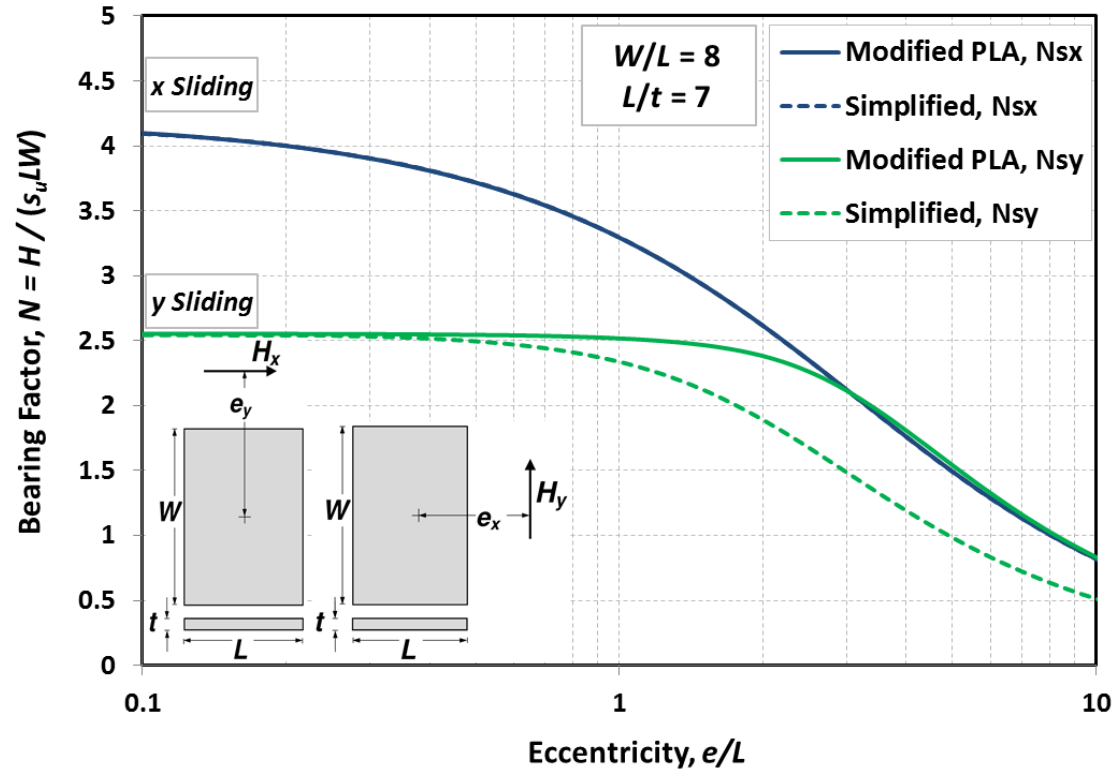

Figure 16- Reduction effect of eccentricity on sliding load capacity for rectangular (W/L=8) plate of $t = L/7$

As discussed in the previous sections, in most cases both simplified and modified PLA solutions over-estimate the FEA predictions with increasing plate thickness except for the simplified solution for rectangular plate under *y*-sliding (Fig. 14). For rectangular plates (i.e. W/L=2, 4 and 8 in Figs. 14-16) under eccentric *x*-sliding the PLA and simplified approaches are essentially yielding the same values. As for the plate bearing capacity under *y*-sliding, the modified PLA predictions show an unconservative trend compared to FEA solutions (Fig. 14), while the simplified solution is on a slightly conservative side.

In general, the modified PLA approach provides a useful tool with minimal computational effort and slightly unconservative yet fairly satisfactory predictions which is expected regarding its upper bound solution and tendency to overestimate the bearing resistance for increased plate thickness. However, the application of simplified method is also advisable, considering the simple and convenient formulation to implement in spreadsheet applications and fairly accurate results. Furthermore, there is no optimization procedure involved in the simplified solution to search for a least upper bound collapse load which offers the simplified solution an advantage over the modified PLA. Note that modified and $PLA_{t=0}$ approaches generate exactly the same yield envelopes for the infinitely thin plates.

***Co-planar shear-torsion* (H_x-H_y-T)**

Figs. 13-16 propose the load capacity for plates under eccentric shear load aligned with the minor and major axis of the plate (i.e. $\psi = 0^\circ$ or 90° with $\gamma = 0^\circ$); thus, the effect of load angle, γ, and other eccentricity angles (ψ) or in other words the general H_x-H_y-T combination is not evaluated. Impact of eccentricity angle (ψ) was partially evaluated in Figs. 13-16. Examining the effect of load angle is also clearly significant since any increase in γ (with constant e and ψ) will

reduce the torsional load, so that for $\gamma = 90^{\circ}$ the torsion yields to zero. Evaluating the effect of load angle, γ, is possible through modified PLA solution (Eqs. 15-24).

The simplified solution is also applicable using the generalized $PLA_{t=0}$ approach (Eqs. 7-10) for infinitely thin plate. The simplified solution also requires the ultimate shear resistance, H_{max}, which is estimated based on a simple formulation summarized in Appendix C.

PLATE UPLIFT CAPACITY UNDER GENERALIZED LOADING

Up to this point, the bearing capacity of plate anchor subjected to combined co-planar shear load and torsion has been studied. Now a question arises that how the combination of shear-torsion loading affects the uplift bearing capacity of the plate anchor.

Throughout the paper, it was well discussed that the plate thickness does not influence the shape of shear-torsion or two-way shear yield envelope in the normalized load space. We also examined the shape of the normalized yield envelopes for normal-shear forces, normal force-moment, and shear force-moment in the API/Deepstar 2D-FE study (Andersen et al. 2004; Murff et al. 2005) for plates of $t=L/20$ to $L/7$. Our evaluations indicated a marginal impact of the plate thickness on the shape of normalized yield surface. Therefore, application of generalized interaction envelope for infinity thin plate could be extended to plate under six degrees of freedom loading. The following mathematical model is adopted to describe the shape of yield envelope for the plate anchor under general loading:

$$f\left(\frac{F_n}{F_{n,\max}},\frac{M_x}{M_{x,\max}},\frac{M_y}{M_{y,\max}},\frac{H_x}{H_{x,\max}},\frac{H_y}{H_{y,\max}},\frac{T}{T_{\max}}\right)=$$

$$\left(\frac{F_n}{F_{n,\max}}\right)^n+\left\{\left(\frac{M_x}{M_{x,\max}}\right)^{mx}+\left(\frac{M_y}{M_{y,\max}}\right)^{my}+\left[\left[\left(\frac{H_x}{H_{x,\max}}\right)^{hx}+\left(\frac{H_y}{H_{y,\max}}\right)^{hy}\right]^h+\left(\frac{T}{T_{\max}}\right)^{mz}\right]^s\right\}^{1/p}-1=0 \quad (26)$$

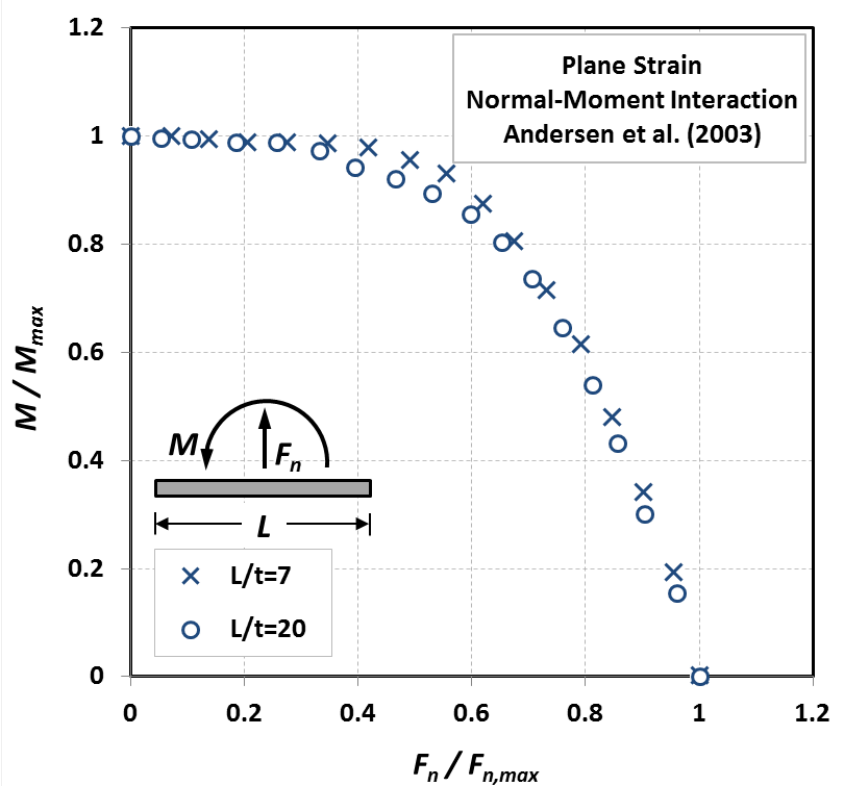
Plane Strain
Normal-Moment Interaction
Andersen et al. (2003)
M / M_max
F_n / F_n,max
M
F_n
L
L/t=7
L/t=20
0
0.2
0.4
0.6
0.8
1
1.2

(a)

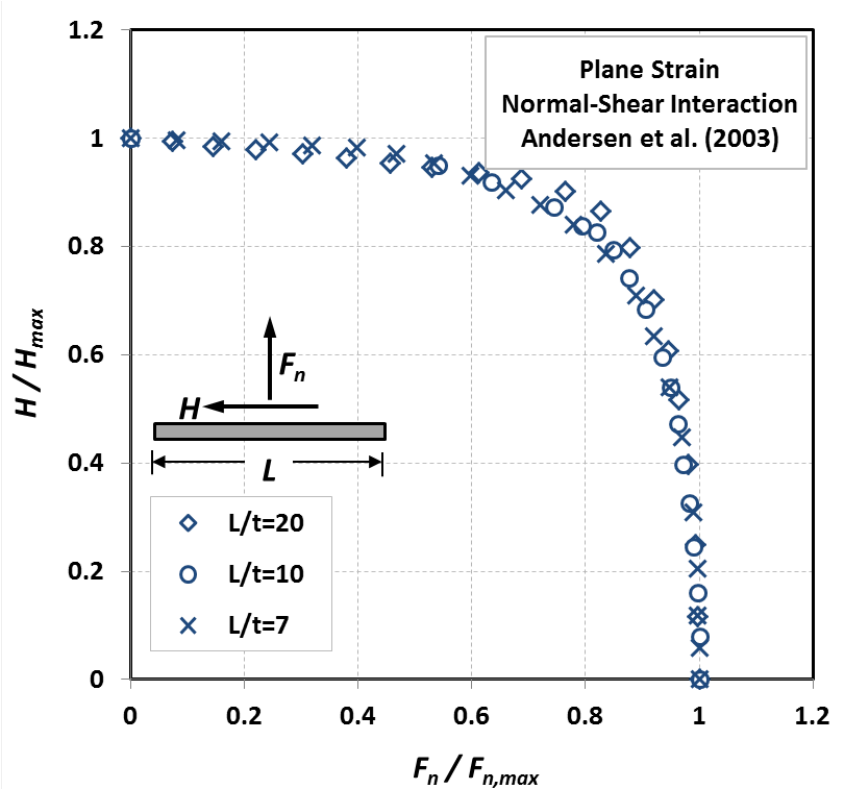
Plane Strain
Normal-Shear Interaction
Andersen et al. (2003)
H / H_max
F_n / F_n,max
F_n
H
L
L/t=20
L/t=10
L/t=7
0
0.2
0.4
0.6
0.8
1
1.2

(b)

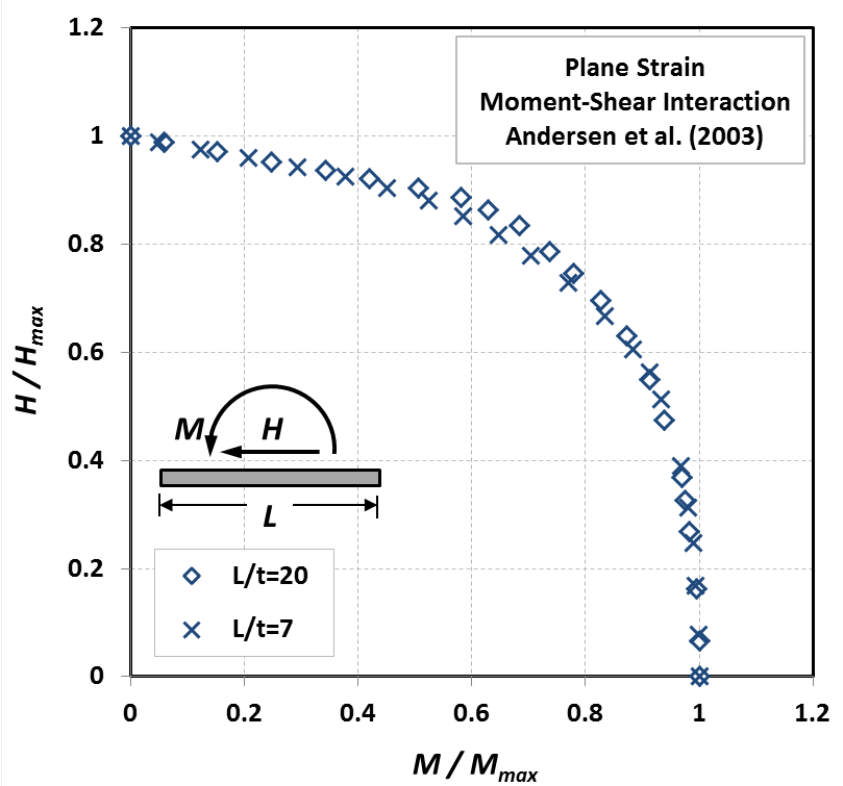

(c)

Figure 17- Yield envelopes for plane strain strip plates of thickness $t=L/20$ to $L/7$ (Andersen et al. 2003): (a) normal-moment; (b) normal-shear; (c) moment-shear

where F_n, H_x, H_y = normal, x-shear, y- shear forces, M_x, M_y, and T: x-moment, y-moment, and torsion components of the generalized combined loading at failure, $F_{n,max}$, $H_{x,max}$, $H_{y,max}$, $M_{x,max}$, $M_{y,max}$, and T_{max} are the corresponding maximum values, and eight constants of n, mx, my, hx, hy, mz, s, and p are the interaction factors.

Regarding the insensitivity of the shape of normalized yield surface to plate thickness, we adopted the same interaction factors proposed in Yang et al. (2010) for the infinitely thin plate. Interaction factors which define the shape of yield envelope are summarized in Table 3. These factors could be used for square and rectangular ($W/L=2$) plates with any arbitrary plate thickness; For other aspect ratios, Interaction factors and maximum capacity values should be evaluated.

Calculation of the bearing capacity for each degree-of-freedom using Eq. 26, requires all the six

447 maximum capacity factors for the desired plate thickness and aspect ratio (rather than available
448 values) to be estimated. The interaction factors for the shear-torsion yield envelope (*hx*, *hy*, and
449 *mz*) are refined regarding the present study.

450 Table 3. Interaction factors for generalized yield envelope

Factors	Square	Rectangular (*W*/*L*=2)
n	3.26	3.20
mx	1.91	1.86
my	1.91	2.47
hx	2.50	2.50
hy	2.50	2.50
h	0.70	0.75
mz	1.75	$1.15+1.23\left[cos\left(\phi\right)\right]^5$
s	3.87	3.75/*mz*
p	1.56	1.93

Notes:

$$f=\left(\frac{F_n}{F_{n,\max}}\right)^n+\left\{\left(\frac{M_x}{M_{x,\max}}\right)^{mx}+\left(\frac{M_y}{M_{y,\max}}\right)^{my}+\left[\left[\left(\frac{H_x}{H_{x,\max}}\right)^{hx}+\left(\frac{H_y}{H_{y,\max}}\right)^{hy}\right]^h+\left(\frac{T}{T_{\max}}\right)^{mz}\right]^s\right\}^{1/p}-1=0$$

ϕ: the angle between line of action of the external force and *y*-axis (ϕ=ψ+γ; Fig. 1)

451 The following relationships and recommendations also can be applied to calculate the maximum
452 capacity values for every six degrees of freedom loading. Note that the weight of plate anchor for
453 typical thickness values available in industry has a negligible effect on the capacity of the anchors:

454 1- Uplift or normal ultimate capacity factor ($F_{n,max}$):

455 The uplift or normal ultimate capacity of the plane strain strip plate anchor could be estimated
456 using the upper-bound derived relationship proposed by O'Neill et al. (2003):

457 $$N_{n,\max}=\frac{F_{n,\max}}{Ls_u}=(3\pi+2)+2\frac{t}{L}\left[\alpha+\frac{1+\alpha}{\sqrt{2}}\right] \quad (27)$$

458 where α is the plate-soil adhesion factor. Table 4 also summarizes the predictions for uplift
459 capacity factor using other effective analytical and numerical approaches for 2D plane stain and
460 3D circular, square, and rectangular plates of different thicknesses.

Table 4. Maximum pure capacity factor for deeply embedded plate anchor

Normal (uplift) bearing capacity ($N_{n,max}$)	2D plane strain Lower bound PLA (Rowe, 1978)	t/L=0; W/L>6: 10.28
	2D plane strain finite element (Elkhatib and Randolph, 2005)	t/L=1/20; W/L>6: 11.62 t/L=1/7; W/L>6: 11.93
	3D upper and lower bound PLA; exact solution (Martin and Randolph, 2001)	t/L=0; Circular[1]: 13.11
	3D large deformation finite element (LDFE) (Wang et al. 2009)	t/L=1/20; Square (W/L=1): 13.17 t/L=1/20; W/L=2: 12.35 t/L=1/20; W/L=4: 11.28 t/L=1/20; W/L=6: 10.95
Moment bearing capacity($N_{M,max}$)	2D finite element, smooth (α=0.0) and rough (α=1.0) strip plates (Elkhatib and Randolph, 2005)	t/L = 1/7: 1.44 and 1.63 for α=0.0 and 1.0 t/L = 1/20: 1.41 and 1.59 for α=0.0 and 1.0
	3D upper bound PLA (Yang et al. 2010)	t/L=0; Circular: $M_{\max} = \pi^2 R^3 s_u \Rightarrow N_{m,\max} = 1.9$
	Calibrated 3D finite element (Yang et al. 2010)	t/L=0; Square (W/L=1): $N_{Mx,\max}$= $N_{My,\max}$=1.9 t/L=0; W/L=2: $N_{Mx,\max}$=2.15; $N_{My,\max}$=1.70

Note:

1- For other plate thicknesses, the pull-out capacity factor for square shaped anchor could be used with reasonable accuracy to calculate capacity factor for circular plates with similar plate area.

All the capacity factors are correct for deeply embedded plates (i.e. H/L or $H/D \geq 6$ where H is the embedment depth, L is the plate shorter length, and D is the diameter of circular anchor). Adopting this assumption means that the failure mechanism is localized around the plate and does not extend to the surface and therefore the bearing capacity is not affected by the effective overburden pressure and soil weight. Thus, the soil is assumed to be a weightless material in the analysis. Also the plate and soil are fully bonded (i.e. no breakaway or separation occurs between plate and soil at the time of failure). Appropriate predictions are provided by Song et al. (2008) and Wang et al. (2010) to evaluate the plate pullout capacity under breakaway/separation condition or when the overburden pressure is influential on the anchor capacity.

2- Moment ultimate capacity factor ($M_{x,max}$, $M_{y,max}$):

O'Neill et al. (2003) used the plane strain upper bound plasticity solution to evaluate the maximum moment capacity factor for a strip plate:

$$N_{M,\max} = \frac{M_{\max}}{L^2 s_u} = \frac{\pi}{2}\left[1+\left(\frac{t}{L}\right)^2\right] \tag{28}$$

The solution could be generalized for square and rectangular plates of finite thickness to calculate moment factors about x and y plate axis using the generalized 2D collapse mechanism in 3D space (Chi 2010):

$$N_{Mx,\max} = \frac{M_{x,\max}}{WL^2 s_u} = \frac{\pi}{2}\left[1+\left(\frac{t}{W}\right)^2\right]\left(\frac{W}{L}\right)\left\{1+\frac{1}{3}\left(\frac{W}{L}\right)\sqrt{1+\left(\frac{t}{W}\right)^2}\right\} \tag{29}$$

$$N_{My,\max} = \frac{M_{y,\max}}{WL^2 s_u} = \frac{\pi}{2}\left[1+\left(\frac{t}{L}\right)^2\right]\left\{1+\frac{L}{3W}\sqrt{1+\left(\frac{t}{L}\right)^2}\right\} \tag{30}$$

Note that the equation for $N_{Mx,max}$ does not provide a good estimates as the W/L increases, probably due to the adopted failure mechanism, while the equation for $N_{My,max}$ works more

481 effectively better, especially for greater W/L. For strip plate (i.e. $W/L \rightarrow \infty$ or $L/W \rightarrow 0$) Eq. (30)
482 yields the O'Neill et al (2003).
483 Some FE and PLA derived solutions for moment capacity factor are also included in Table 4 for
484 2D plane stain and 3D circular, square, and rectangular plates of different thicknesses.
485 3- Parallel or shear ultimate capacity factor ($N_{sx,max}$, $N_{sy,max}$):
486 As discussed previously, the limit equilibrium equations (Eqs. 2-3) provide simple yet fairly
487 accurate predictions.
488 4- Torsional ultimate capacity factor ($N_{t,max}$):
489 The closed form solution developed based on limit equilibrium solution (Eqs. 5-6) with factor of
490 C_f=0.67 provides a fairly accurate and simple estimation for the torsional maximum capacity.

CONCLUSIONS

The focus of this study is to offer a modified upper bound plastic limit analysis (PLA) as well as a simplified baseline solution based on the limit equilibrium and virtual work approaches for general conditions of shear-torsional loading. This study also evaluates the effect of eccentric shear forces on the uplift capacity of a plate anchor under six-degrees-of-freedom generalized loading. This study indicates the following:

1. Eccentricity reduces the plate shear and consequently uplift capacities. The reduction begins to become significant (>5% of reduction in shear capacity) in square plates at eccentricity levels of $e>0.1L$ (Fig. 8). For perspective, an eccentricity $e/L = 0.5$ - a load applied at the edge of a square plate - reduces shear capacity by more than 40%.
2. Plates of higher aspect ratio (W/L) are less susceptible to uplift capacity reduction due to planar eccentric loading. Reduction in uplift capacity due to eccentricity of in-plane shear loading is always more significant for shear loading parallel to the short axis of the plate.
3. The proposed baseline solutions to calculate the pure shear capacity, limit equilibrium Eqs. 2 and 3, offer fairly accurate predictions for plate under pure shear loading (Fig. 9). The limit equilibrium derived Eq. 5, to estimate pure torsional capacity for theoretical infinitely thin plate ($t = 0$), is accurate as well. For plates of finite thickness ($t > 0$), Eq. 6 offers the increase in torsional capacity induced by plate thickness which can provide reasonably accurate solutions if used in combination with a correction factor $C_f = 0.67$.
4. The proposed modifications in PLA formulation for plate under combined two-way translation-torsion, significantly improves the Yang et al. (2010) PLA predictions both in terms of “size” (i.e. pure capacity values) as well as the “shape” (i.e. interaction response) of the two-way shear and shear-torsion yield envelopes. Predictions of the proposed

514 modified PLA approach for the shape of shear-torsion yield envelope in normalized load
515 space generally agree well with FEA predictions (Figs. 10-12). However, the method
516 generally over-predicts the increase in pure torsional resistance associated with increased
517 plate thickness, *t* (Tables 1 and 2; Fig. 9, and Figs. 13-16). Application of the modified
518 PLA approach is therefore advisable when the obtained normalized yield envelope is
519 used in combination with the FEA derived or corrected pure torsional capacity (Eqs. 5
520 and 6) and pure shear capacity (Eqs. 2-3).

521 5. The general insensitivity of the shape of the shear-torsion yield loci to plate thickness *t*
522 (Figs. 10-12) offers the opportunity to develop a simplified analysis in which fairly
523 accurate analytical expressions for shear resistance (Eqs. 2 and 3) are used in conjunction
524 with a virtual work analysis for zero thickness plate ($PLA_{t=0}$: Eqs. 6-10) to predict the
525 reduction in capacity due to eccentricity. The method is fairly robust, as it requires no
526 find a least upper bound. Predictions from the simplified method provide reasonable
527 conservative estimates of the reduction in *y*-shear resistance induced by eccentricity,
528 however similar to modified PLA approach the reduced *x*-shear capacity factors will be
529 over-predicted by the simplified approach, thus the results should be used with caution.

530 6. Reviewing the normalized yield envelope for plate anchor under other combinations of
531 loading indicates the insensitivity of the normalized yield surface for a plate under
532 generalized six-degrees-of-freedom loading to the plate thickness (Figs. 10-12, Fig. 17).
533 Thus, to evaluate the uplift capacity reduction of a plate under any load combinations, the
534 normalized yield surface for an infinitely thin plate (Eq. 17, Table 3) could be used in
535 combination with the ultimate capacity factors available in the current study and literature
536 (Table 4).

537 **Appendix A. Energy Dissipation Rate Terms for PLA (Fig. 2)**

Ref.	Mechanism	Location	Equation
Yang et al. (2010) formulation	Slip at the edges of the plate	Sides AD and BC	$\dot{D}_{e(AD,BC)} = \int_{-W/2}^{W/2} s_u \dot{\beta}\left[2N_e\left\|y-y_0\right\| + \alpha\left\|L/2-x_0\right\| + \alpha\left\|L/2+x_0\right\|\right]tdy$
		Sides AB and CD	$\dot{D}_{e(AB,CD)} = \int_{-L/2}^{L/2} s_u \dot{\beta}\left[2N_e\left\|x-x_0\right\| + \alpha\left\|W/2-y_0\right\| + \alpha\left\|W/2+y_0\right\|\right]tdx$
	Slip at the top and base of plate ABCD	Base and top	$\dot{D}_s = 2\int_{-W/2}^{W/2}\int_{-L/2}^{L/2} \alpha s_u R(x,y)\dot{\beta}dxdy$
Current study (Modified PLA)	Slip at the edges of the plate	Sides AD and BC	$\dot{D}_{e,BC} = \int_{-W/2}^{W/2} s_u \dot{\beta}\left(N_{st}\left\|\frac{L}{2}-x_0\right\| + N_{nt}\left\|y-y_0\right\|\right)tdy$ $\dot{D}_{e,AD} = \int_{-W/2}^{W/2} s_u \dot{\beta}\left(N_{st}\left\|\frac{L}{2}+x_0\right\| + N_{nt}\left\|y-y_0\right\|\right)tdy$ $\begin{cases} N_{st} = N_{st,\max}\left[\left(\frac{N_{nt,\max}}{N_{st,\max}}\cdot\frac{\left\|x-x_0\right\|}{\left\|y-y_0\right\|}\right)^2+1\right]^{-0.5} \\ N_{nt} = \left(\frac{N_{nt,\max}}{N_{st,\max}}\right)^2\left(\frac{\left\|x-x_0\right\|}{\left\|y-y_0\right\|}\right)N_{st} \end{cases}$ where: $x = L/2$ for BC; $x = -L/2$ for AD
		Sides AB and CD	$\dot{D}_{e,AB} = \int_{-L/2}^{L/2} s_u \dot{\beta}\left(N_{st}\left\|\frac{W}{2}-y_0\right\| + N_{nt}\left\|x-x_0\right\|\right)tdx$ $\dot{D}_{e,CD} = \int_{-L/2}^{L/2} s_u \dot{\beta}\left(N_{st}\left\|\frac{W}{2}+y_0\right\| + N_{nt}\left\|x-x_0\right\|\right)tdx$ $\begin{cases} N_{st} = N_{st,\max}\left[\left(\frac{N_{nt,\max}}{N_{st,\max}}\cdot\frac{\left\|y-y_0\right\|}{\left\|x-x_0\right\|}\right)^2+1\right]^{-0.5} \\ N_{nt} = \left(\frac{N_{nt,\max}}{N_{st,\max}}\right)^2\left(\frac{\left\|y-y_0\right\|}{\left\|x-x_0\right\|}\right)N_{st} \end{cases}$ where: $y = W/2$ for AB; $y = -W/2$ for CD
	Slip at the top and base of plate ABCD	Base and top	$\dot{D}_s = 2\int_{-W/2}^{W/2}\int_{-L/2}^{L/2} \alpha s_u R(x,y)\dot{\beta}dxdy$ [Same as Yang et al. (2010)]

Notes:

(x_0, y_0): coordinates of the center of rotation (Fig. 2)

(x_f, y_f): coordinates of the application point for the external force H (Fig. 2)

s_u: undrained shear strength of the soil

L and W: Length and width of the plate anchor parallel to x and y axis respectively

α: adhesion factor

$\dot{\beta}$: virtual rate of rotation

N_e: plane strain bearing capacity factor equal to 7.5

$R(x,y):\sqrt{(x-x_0)^2+(y-y_0)^2+(t/2)^2}$

N_{st}: normalized shear force acting along the plate edge

N_{nt}: normalized force acting perpendicular to the plate edge

$N_{st,max}$: maximum normalized shear force acting along the plate edge

$N_{nt,max}$: maximum normalized force acting perpendicular to the plate edge

y constant for the sides AB (y=W/2) and CD (y=-W/2)

x constant for the sides BC (x=L/2) and AD (x=-L/2)

APPENDIX B. Integration of dissipation rate for *d*=0 analysis

Analytical evaluation of the inner integral in Eq. 12 is possible to permit a single numerical integration. The resulting expression is:

$$\dot{D} = 2s_u\dot{\beta}\int_{-W/2}^{W/2}\left[(a_1c_1 - a_2c_2) + y^2\ln\left|\frac{a_1+c_1}{a_2+c_2}\right|\right]dy$$
$$a_1 = \rho_{opt} + L/2$$
$$a_2 = \rho_{opt} - L/2 \qquad \text{(B-1)}$$
$$c_1 = \sqrt{a_1^2 + y^2}$$
$$c_2 = \sqrt{a_2^2 + y^2}$$

Eq. B-1 can be integrated between the limits -*W*/2 to *W*/2 using classical numerical integration formulas.

APPENDIX C. Estimation of H_{max} for the simplified solution

For a plate anchor subjected to horizontal load of H (Fig. 1), these relationships are valid:

$$\left(\frac{H_x}{H_{x,\max}}\right)^{hx}+\left(\frac{H_y}{H_{y,\max}}\right)^{hy}-1=0$$

$$H_x = H.\sin(\phi) \qquad \text{(C-1)}$$
$$H_y = H.\cos(\phi)$$

where ϕ is the angle between line H and y-axis (i.e. ϕ=ψ+γ in Fig. 7). $H_{x,max}$ and $H_{y,max}$ are estimated by the limit equilibrium derived equations for pure translational load capacity using Eqs. 2 and 3 which proved to be fairly accurate. As discussed previously in the paper, application of the FE derived hx=hy=2.5 offers a fairly accurate estimate for the shape of N_{sx}- N_{sy} yield envelope. Therefore, H for the simplified solution is evaluated using the following equation:

$$H=\left[\left(\frac{\sin(\phi)}{H_{x,\max}}\right)^{2.5}+\left(\frac{\cos(\phi)}{H_{y,\max}}\right)^{2.5}\right]^{-0.4} \qquad \text{(C-2)}$$

REFERENCES

Andersen, K.A., Murff, J.D. & Randolph, M.F. (2004). “Deepwater Anchor Design Practice-Vertically Loaded Drag Anchors”, *Phase II Report to API/Deepstar JIP*, Volume III.

Aubeny, CP, Murff, JD and Roesset JM (2001). “Geotechnical issues in deep and ultra deep waters,” *International Journal of Geomechanics.* Vol. 1, No. 2, pp. 225-247

Chen, WF, and Liu, XL (1990). *Limit analysis and soil plasticity*. Elsevier Publishing Co., Amsterdam, The Netherlands.

Chi, Ch (2010). *Plastic limit analysis of offshore foundation and anchor*. Doctoral dissertation, Texas A&M University.

Elkhatib, S, and Randolph, MF (2005). “The effect of interface friction on the performance of drag-in plate anchors,” *Proc. Int. Symp. On Frontiers in Offshore Geotechnics, IS-FOG05,* Perth, pp. 171-177.

Martin, CM, and Randolph, MF (2001). “Applications of the lower and upper bound theorems of plasticity to collapse of circular foundations,” *Proc. 10th Int. Conf. Int. Association of Computer Methods and Advances in Geomechnics,* Tucson, 2, pp. 1417-1428.

Murff, JD, Aubeny, CP, Yang, M (2010). “The effect of torsion on the sliding resistance of rectangular foundations,” *Proc. 2nd Int. Symp. on Frontiers in Offshore Geotechnics (ISFOG),* Perth, Australia, pp. 439-444.

Murff, JD, Randolph, MF, Elkhatib, S, Kolk, HJ, Ruinen, RM, Strom, PJ, and Thorne, CP (2005). “Vertically loaded plate anchors for deepwater applications,” *Proc. Int. Symp. on Frontiers in Offshore Geotechnics: ISFOG 2005,* Perth, Australia, pp. 31-48.

Nouri, H, Biscontin, G, Aubeny, C (2014). “Undrained bearing capacity of shallow foundations under combined sliding and torsion,” A*SCE Journal of Geotechnical and Geoenvironmetal*

Engineering. Vol. 140, No. 8.

Nouri, H (2013). *Numerical Methods in Offshore Geotechnics: Applications to Submarine Landslides and Anchor Plates*. Doctoral dissertation, Texas A&M University.

O'Neill, MP, Bransby, MF, and Randolph, MF (2003). "Drag anchor fluke-soil interaction in clays," *Canadian Geotechnical Journal*, vol. 40, pp. 78-94.

Prager, W (1959). *An Introduction to Theory of Plasticity*. Addison Wesley: Reading, MA.

Rowe, RK. (1978). "Soil-structure interaction analysis and its application to the prediction of anchor behavior," PhD thesis, University of Sydney, Sydney, Australia.

Song, Z, Hu, Y, and Randolph, MF (2008). "Numerical simulation of vertical pullout of plate anchors in clay," *ASCE Journal of Geotechnical and Geoenvironmenal Engineering*. Vol. 134, No. 6, pp. 866-875.

Tan, F (1990). *Centrifuge and theoretical modelling of conical footings on sand*. Ph.D. thesis, The University of Cambridge, Cambridge, U.K.

Wang, D, Hu, Y, and Randolph, MF (2010). "Three-dimensional large deformation finite element analysis of plate anchors in uniform clay," *ASCE Journal of Geotechnical and Geoenvironmenal Engineering*. Vol. 136, No. 2, pp. 355-365.

Yang, M, Murff, JD, and Aubeny, CP (2010). "Undrained Capacity of Plate Anchors under General Loading," *ASCE Journal of Geotechnical and Geoenvironmental Engineering*. Vol. 136, No. 10, pp. 1383-1393.